

Cretaceous volcanic reservoirs and their exploration in the Songliao Basin, northeast China

Pujun Wang and Shumin Chen

ABSTRACT

Major reservoirs in the Songliao Basin (SB) are composed of volcanic rocks below 3000 m (9843 ft) of buried depth. Gas accumulations are mostly found in the buried volcanic highs, which in general correspond to paleovolcanic centers. Porosity in the volcanic rocks depends on both primary and secondary processes. The best porosity is preferentially developed in a proximal facies near the central part of each volcanic edifice. Porosity and permeability decrease with depth of burial for both volcanic and non-volcanic sections, but their porosity-depth trends differ. Lava and welded ignimbrite slowly lose porosity with burial depth because they solidified by cooling, and their groundmasses ($\geq 75\%$) are poor in quartz and calcite precipitation, thus preserving porous space. In contrast, the associated sandstone, conglomerate, tuff, and tuffite are more sensitive to overburden pressure, suffering more intense compaction and cementation. As a result, porosity and permeability of lava and ignimbrite exceed that of the other rocks, and thus, they are the best reservoir rocks below burial depths of ca. 3000 m (9843 ft) in the SB. The paleovolcanic domes are rich in both lava rocks and fractures of diverse origin, and the topographic highs provide favorable locations for gas migration and accumulation.

INTRODUCTION

Volcanic reservoirs have been found worldwide. The lithologies range from basalt to andesite or rhyolite formed in various geological ages (Schutter, 2003). Commercial Cenozoic–Mesozoic volcanic reservoirs commonly occur in Pacific Rim areas, such

AUTHORS

PUJUN WANG ~ College of Earth Sciences, Jilin University, Changchun 130061, China; wangpj@jlu.edu.cn

Pujun Wang was born in 1959 in Heilongjiang. He obtained his B.S. and M.S. degrees and Ph.D. in geosciences at Jilin University in 1982, 1989, and 1994. He was at Tübingen University in Germany as a research fellow at AvH Foundation from 1999 to 2000. He has held a professional position since 1982 and became a full professor in 1996 at Jilin University.

SHUMIN CHEN ~ Institute of Exploration and Development of Daqing Oilfield Company Ltd., Daqing 163712, China; Chenshumin@petrochina.com.cn

Shumin Chen was born in 1962 in Inner-Mongolia. He obtained his B.S. degree and Ph.D. in geophysics and petroleum geology at Jilin University in 1985 and 2000. He has been working in petroleum exploration at Daqing Oilfield Company since 1985, and now he is the deputy director of the E & D Research Institute of the company.

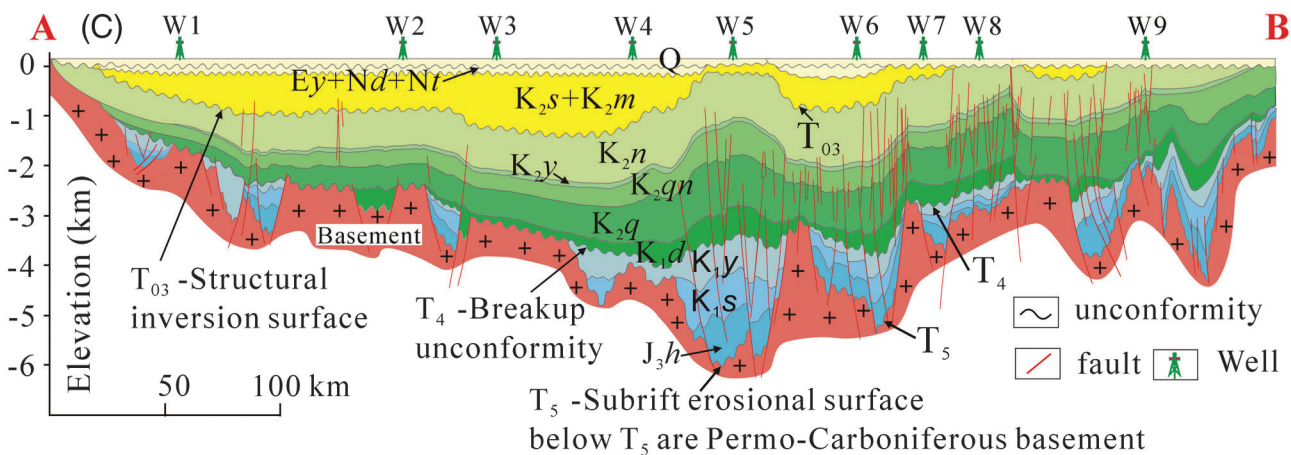
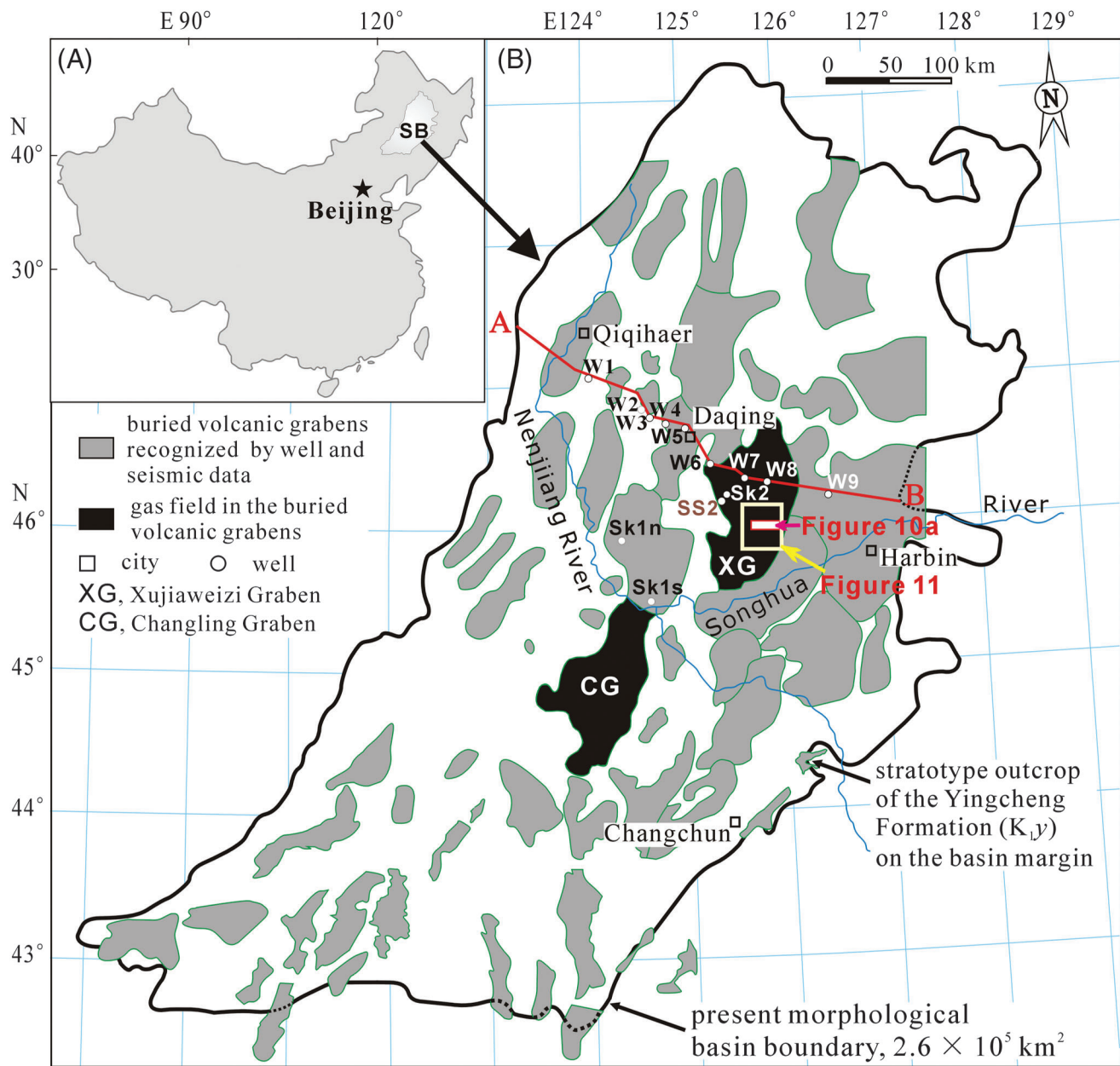
ACKNOWLEDGEMENTS

This project was sponsored by MOST (Grant 2009CB219300 and 2012CB822000) with assistance from the EPLENEA key lab of China Education Ministry. Thanks to W. H. Bian, Y. F. Gao, H. F. Tang, Y. L. Huang, C. J. Jiang, C. Y. Chen, and Y. X. Wu for their contributions toward field work, core and thin section descriptions, and data processing. Thanks also to F. Mattern, R. P. Sorenson, J. Witte, N. W. Hayman, and J. K. Geslin for their constructive comments on the manuscript. We also thank J. T. Parrish for carefully reviewing the paper before submission and an anonymous referee for comments about diagenesis of interbedded volcanogenic and sedimentary rocks.

Copyright ©2015. The American Association of Petroleum Geologists. All rights reserved.

Manuscript received May 31, 2013; provisional acceptance April 23, 2014; revised manuscript received June 21, 2014; final acceptance September 4, 2014.

DOI 10.1306/09041413095



as China, Japan, and Argentina (e.g., Chen et al., 1999; Magara, 2003; Sruoga and Rubinstein, 2007). Lavas can in some cases show the highest porosity but the lowest permeability in a volcanogenic succession (Lenhardt and Götz, 2011). The question still remains as to how volcanic rocks gain better porosity and permeability than their surrounding sedimentary rocks.

Cretaceous volcanogenic successions are widely distributed within and around the Songliao Basin (SB) (Figure 1) at depths in the range 1700 to 6200 m (5577 to 20,341 ft) as revealed by exploration drilling (Figure 2). Volcanic reservoirs are usually found below 3000 m (9843 ft), whereas sedimentary reservoirs dominate at shallower depths. Therefore, the Songliao Basin provides an opportunity to understand why different types of reservoirs tend to develop at different depths.

Recently, more than 300×10^9 m³ of natural gas (ca. 2×10^9 bbl oil equivalent) have been proven in the Xujiaweizi graben (Figure 1). Most of the gases are hosted in the Lower Cretaceous volcanic reservoirs (Feng, 2008), although the volcanogenic successions contain other types of rocks, including sedimentary rocks and tuffite (Figure 3). In recent years, nearly 400 wells have been drilled targeting the volcanic reservoirs. With a methane content of 58% to 99%, the hydrocarbon gases hosted in the volcanic rocks are mainly of the coal-type gases, although some may be mixed with oil-type or even mantle-derived gases (Xu et al., 1995; Huang et al., 2004; X. B. Wang et al., 2009). Although the charging history of natural gases was complicated, the main episode of accumulation occurred during the mid-Cretaceous (C. Q. Li et al., 2006). Porosity in the volcanic reservoirs comprises both pores and fractures. Although 15 lithofacies have been recognized, only 4 of them tend to develop effective volcanic reservoirs (e.g., Wang et al., 2003). The term effective indicates that the reservoirs contain gas, water, or a mixture of both, coupled with the

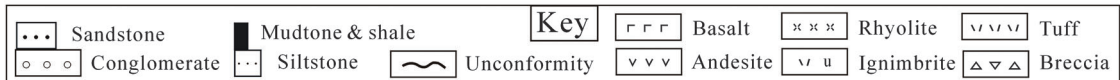
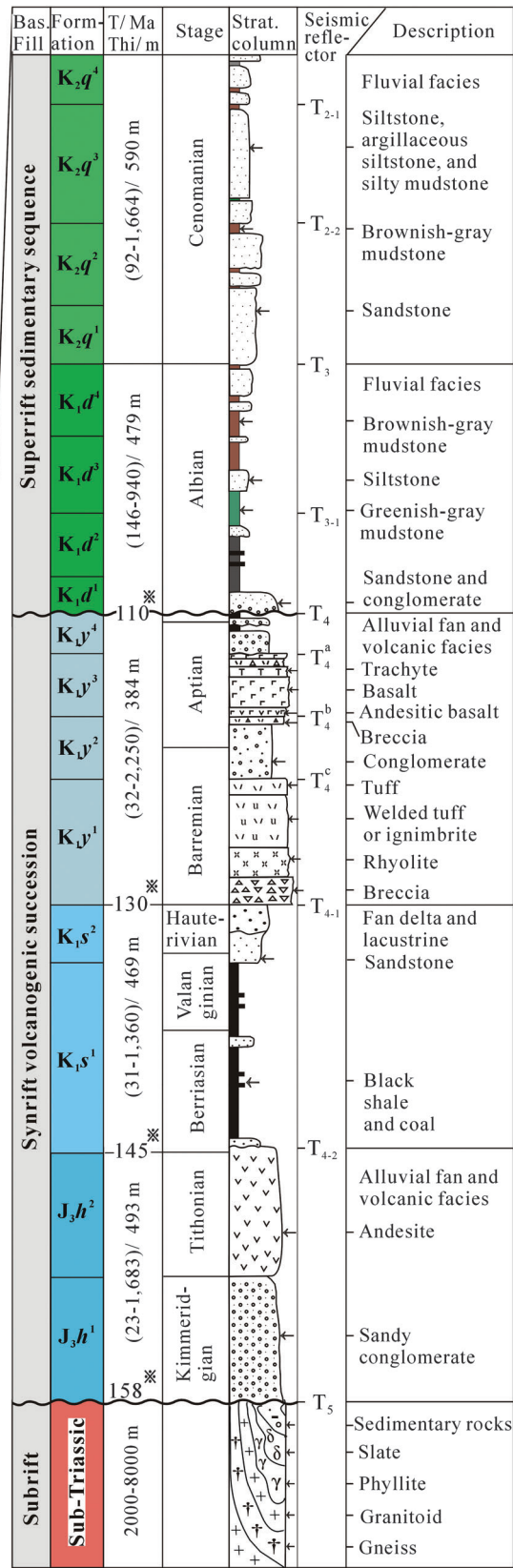
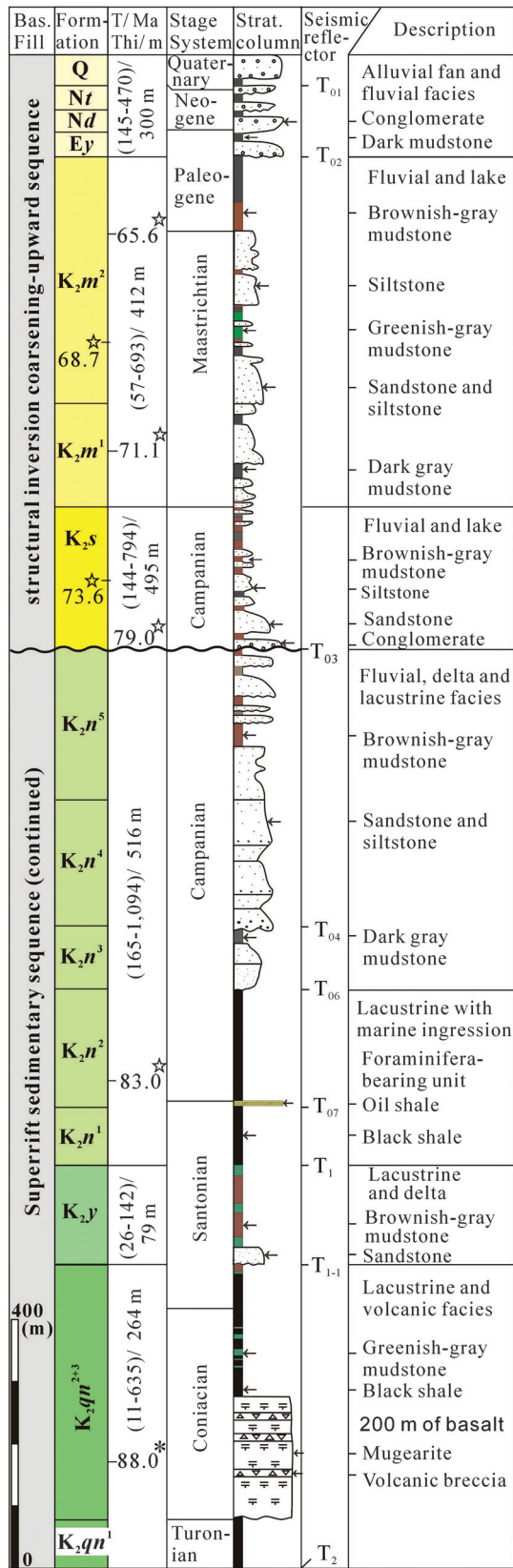
sufficient permeability to permit flow as confirmed by drilling.

Despite progress in the understanding of volcanic reservoirs mentioned previously, some key phenomena remain problematic. Among them are (1) the contrasting overburden effect on lava and welded ignimbrite with higher porosity and better permeability compared to sedimentary rocks, tuff (unwelded), and tuffite below a depth of about 3000 m (9843 ft) and (2) the reason for the predominant occurrence of effective volcanic reservoirs in the central parts of the paleovolcanoes. The objective of this paper is not to provide a comprehensive review of the SB volcanic reservoirs but instead to (1) characterize and explain the volcanic and associated reservoir rocks below 3000 m (9843 ft) of burial depth, (2) analyze the controlling factors for the formation of an effective volcanic reservoir, and (3) share exploration experience of volcanic rocks. The results of this work have implications for further development of deep SB targets and, possibly, for volcanic rock petroleum plays elsewhere (e.g., Tomaru et al., 2009; Witte et al., 2012).

DATA, METHODS, AND TERMS USED

Seismic data, well logs, drill cores, and cuttings data used in this paper were obtained during exploration of the SB. Volcanic borehole sections totalling 53,649 m (33 mi) from 173 wells were used in this study. Over 10,000 rock samples from drill cores and cuttings, as well as outcrops, have been studied for lithology, facies, and diagenesis using thin-section analysis by the authors' working group since 1996. The results provide a major database for the statistical research in this paper. Porosimeter porosity and permeability were analyzed in the laboratory of E & D Institute of Daqing Oilfield Company on samples from borehole cores (1799 specimens) and shallow

Figure 1. (A) Location of the Songliao Basin (SB), northeast China. (B) Distribution of volcanic grabens within and around the SB. (C) Cross section of the basin fill drawn through A–B. Note that the volcanic grabens are stratigraphically bounded between two seismic reflectors: T₅, the subrift erosional surface, and T₄, the breakup unconformity. They are covered by the superrift sedimentary sequence as shown in Figure 2. The seismic reflectors (T₅, T₄, and T₀₃) and formation symbols such as K_{1y} correspond to those in Figure 2. Stratigraphic boundaries were identified by well logs coupled with core sections from boreholes. Fault, graben, and stratigraphic correlations were interpreted by borehole-constrained two-dimensional and three-dimensional seismic data.



drill cores (156 specimens), as listed in Tables 1 and 2. The latter specimens were collected from two sub-surface boreholes on the basin margin, each 255 m (837 ft) deep. Core recovery was 95% from the marginal stratotype outcrop of the Yingcheng Formation (K_{1y}). For a reasonable comparison between shallow and deep borehole samples, samples of the same lithology were selected from both within and on the margin of the SB (Figure 1). The two groups of samples originate from equivalent stratigraphic horizons based on their lithologic associations, stratigraphic locations, isotopic ages, and fossil assemblages contained in the sedimentary intercalations (Wang et al., 2002a, b). Thus, the samples in Table 2 are suitable for comparison because they are similar except for their burial depths. Young's moduli of the SB samples were determined in the laboratory of the Chinese Academy of Geosciences with the sonic speed test system of American Tektronix Company at laboratory conditions (temperature = 25°C, pressure = 1 atm) using cylindrical specimens (diameter = 25 mm, height \geq 50 mm).

Image analysis was used for counting pores and fractures in the volcanogenic rocks. The specimens are from high-resolution photographs taken on outcrops (Figure 4p1, m1), drill cores (Figure 4p6, m2–m4), and thin sections impregnated with colorful dye-stained resin (e.g., Figure 4p7). These two kinds of reservoir pore spaces were counted separately using computer software of CoreDBMS designed by Daqing Oilfield Company. Pores and fractures are defined by different colors. The computer can recognize and count each of them separately. Resolution of the image analysis depends on both specimen quality and the number of camera pixels. Those pore spaces with apertures larger than 20 μm are under the microscope as shown in Figure 4p7. Pore and

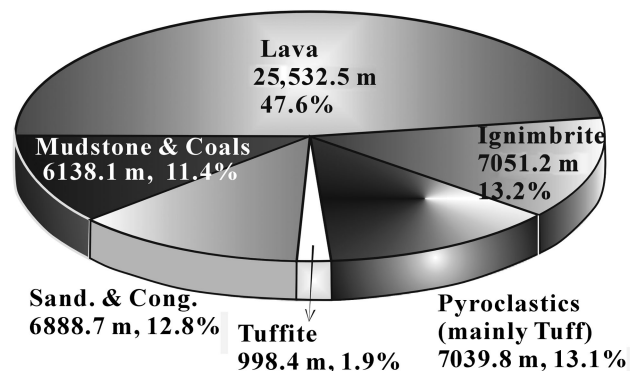


Figure 3. Total thickness and corresponding volume percent of constituent rocks in the Yingcheng Formation (K_{1y}) based on 53,649 m (33 mi) of volcanogenic sections from 173 boreholes. The lava is composed of rhyolite and dacite (64%), andesite (20%), and basalt (16%), respectively.

fracture contributions to bulk porosity are listed in Table 3.

Lithologic definitions are based on LeMaitre (1989), Jackson (1997), and Einsele (2000, p. 64–74) with only minor modifications: (1) lava: volcanic rocks that solidified from molten extrusives by cooling; (2) welded ignimbrite or ignimbrite: fragment-bearing, welded volcanic rocks that solidified by cooling and in some cases by compaction; (3) pyroclastic rocks or pyroclastics: consolidated by compaction with more than 75% pyroclasts; (4) tuff: volcanic ash consolidated by compaction; and (5) tuffite: mixed pyroclasts and epiclasts with 25% to 75% pyroclastic material.

It should be noted from the definitions above that diagenesis of lava and welded ignimbrite is temperature controlled in that most lithification occurs immediately after the magma cools at the Earth's surface. For the other rocks, overburden pressure largely controls induration and stiffness, which gradually increase with increasing burial depth (Figure 5).

Figure 2. Upper Mesozoic stratigraphic column for the Songliao Basin, showing three cycles of basin fill, (1) synrift, (2) superrift, and (3) structural inversion. Volcanic reservoirs are predominantly developed in the Lower Cretaceous Yingcheng Formation (K_{1y}), which is just above the major source rocks in the Shahezi Formation (K_{1s}). The vertical succession, thickness, and fossils are based on the stratigraphic sequences drilled through by wells like SK1n and SK1s (cf. Figure 1) (Gao et al., 2009; Xi et al., 2011). The top right superscripts in the second column, such as in K_{1y}^1 , indicate members in each formation. Vertical numbers such as (32–2250)/384 m in the third column indicate borehole statistical data on formation thickness: (minimum–maximum)/mean. Isotopic ages in the second and third columns are from Wang et al. (2002a, 2007a, those with \otimes), P. J. Wang et al. (2009, with \ast), and Wang et al. (2014, those with \star), respectively. Stage and system in the fourth column are based on the International Chronostratigraphic Chart of International Commission on Stratigraphy, January 2013.

Table 1. Statistical Data for Porosimeter Porosity (%) and Permeability (millidarcys) Corresponding to Figure 6

	Volcanogenic Rocks			Sedimentary Rocks	
	Lava	Ignimbrite	Pyroclastics	Sand./Cong.	Combined
Porosity (Max–Min) mode/ median/arithmic mean	(21.9–0.3) 7.0/5.7/6.5	(20.1–0.2) 6.0/6.0/6.7	(14.2–0.2) 6.0/6.7/6.4	(30.5–0.6) 8.0/9.84/10.0	(30.5–0.2) 6.0/7.9/8.6
Permeability (Max–Min) mode/median/geometric mean	(94.4–0.003) 0.04/0.059/0.08	(33.9–0.003) 0.03/0.043/0.06	(27.0–0.004) 0.03/0.045/0.07	(2999.4–0.002) 0.3/1.36/1.37	(2999.4–0.002) 0.05/0.308/0.38
Number of samples	301	307	155	1036	1799

As demonstrated here, diagenesis of lava and welded ignimbrite is primarily temperature controlled. This is similar to porosity destruction in many tight gas sandstones, where initial porosity is reduced by compaction, but further porosity loss is dominated by the accumulation of cementing material controlled by thermal history (Lander et al., 2008).

OVERBURDEN PRESSURE EFFECT

Reservoir and mechanical parameters vary with burial depth for different kinds of rocks in the SB. Lava and welded ignimbrite are significantly different from sedimentary and pyroclastic rocks in that their Young's modulus is less influenced by overburden pressure (Figure 5A). In contrast, Young's modulus for sedimentary and pyroclastic rocks increases significantly with burial depth (Figure 5B, C) in the range 2500–5000 m (8202–16,404 ft). Porosimeter porosity and permeability decrease with increasing depth for all rocks, but each rock shows its own specific trend (Figures 6–8).

Comparisons between Volcanic and Sedimentary Rocks

The comparison between volcanic and sedimentary rocks is focused on the changes in porosity and permeability with buried depth. Porosity and permeability versus depth curves (Figure 6) compare the burial behaviors of different kinds of rocks. Two groups can be identified from the curves: (1) sedimentary rocks including sandstone and conglomerate and (2) volcanic rocks including lava and ignimbrite. Pyroclastic rocks are between the previously two

mentioned groups, as discussed in the following section. Figure 6 shows that porosity and permeability of the sedimentary rocks show a sharp decline between 1000 and 3000 m (3281 and 9843 ft). Below 3000 m (9843 ft), both porosity and permeability decrease slightly and show generally low values. In contrast, porosity and permeability of the volcanic rocks are rather independent of depth. As a result of these two different trends, volcanic rocks have generally greater porosity and permeability than sandstones and conglomerates below ~3000 m (9843 ft) depth.

Comparison among Volcanogenic Rocks

Lava, welded ignimbrite, and pyroclastics respond differently to burial depth with regard to porosity and permeability. Pyroclastic rocks have textures similar to sandstones in that they are both composed of clasts and matrix. Moreover, tuffs are good reservoir rocks in some volcanic basins of northeast Asia (e.g., Levin, 1995; Tomaru et al., 2009). In the SB, pyroclastic rocks were principal targets for petroleum plays from 1996 to 2000. Production showed that their porosity or permeability was poor and often close to the minimum limit for effective gas reservoirs (3% or $0.01 \times 10^{-3} \mu\text{m}^2$), which led to diminishing interest in these targets. The poor reservoir quality mainly results from dense compaction coupled with subsequent cementation of the pyroclastics (Figure 9D, Table 4).

For samples from the surface to 4214 m (13,825 ft) depth (Table 2 and Figures 7, 8), both porosity and permeability decrease for all three types of volcanogenic rocks. However, the trends are significantly different. Lavas show the slowest decrease,

Table 2. Comparison of Porosimeter Porosity and Permeability vs. Buried Depth for Lava, Ignimbrite, and Pyroclastics, and Between Shallow and Deep Samples for the Same Lithology. Data Correspond to Figures 7 and 8

Litho-Type	Sample Source	Buried Depth (m)	Sample Number	Porosimeter Porosity (%)					Porosimeter Permeability (millidarcys)				
				Min	Max	Mode	Median	Arithmetic Mean	Min	Max	Mode	Median	Geometric Mean
Lava	Margin*	1.6–187.8	113	0.3	34.8	15.0	15.4	15.0	0.01	670	0.10	0.15	0.18
	Basin	2884–4214	249	0.3	21.9	5.5	6.6	7.4	0.004	17.3	0.04	0.05	0.08
	Ratio of Shallow/Deep			1	1.6	2.7	2.3	2	2.5	38.73	2.5	3	2.25
Ignimbrite	Margin*	82–254	11	10	25	17	19.6	18.6	0.03	7.29	0.30	0.24	0.21
	Basin	3323–3733	300	0.2	15.6	7.0	6.7	6.4	0.002	5.33	0.06	0.04	0.05
	Ratio of Shallow/Deep			50	1.6	2.4	2.9	2.9	15	1.37	5	6	4.2
Pyroclastics	Margin*	88–249	32	9.9	32.8	21	20.85	20.1	0.02	75.5	0.60	0.58	0.65
	Basin	2925–4027	62	0.7	14.3	2.5	3.5	4.6	0.004	4.64	0.02	0.02	0.03
	Ratio of Shallow/Deep			14.1	2.3	8.4	6	4.4	5	16.27	30	29	21.67

*Note: Margin samples were collected from two shallow subsurface boreholes drilled on stratotype outcrop of the Yingcheng formation (K₁y) on the southeast margin of the Songliao Basin. Basin samples are from the buried grabens of Xujiawezhi graben and Changling graben in Figure 1.

whereas pyroclastics display the fastest decrease from shallow to greater depth. The difference of both porosity and permeability between shallow and deep samples increases systematically from lava to ignimbrite to pyroclastics (Figure 8), indicating an increasing impact of overburden pressure on their reservoir parameters. The intersection between the porosity lines occurs at 2500 m (8202 ft) depth. The corresponding rock permeability shows similar trends, but the intersection is shallower at about 2000 m (6562 ft) depth, as shown in Figure 7. The ratios of mean value from shallow to deep samples indicate similar trends (Table 2), that is, the ratios of permeability are significantly higher than the corresponding ratios of porosity. Permeability ratios are 2.3, 4.2, and 21.7, and the corresponding porosity ratios are 2.0, 2.9, and 4.4 for lava, ignimbrite, and pyroclastics, respectively.

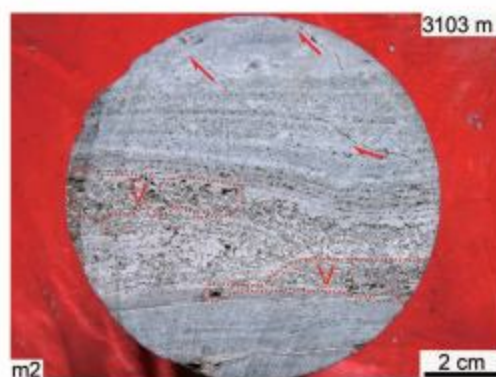
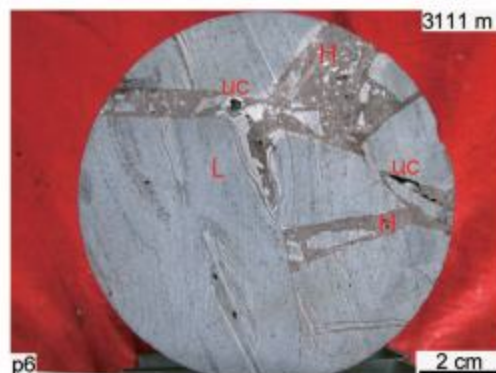
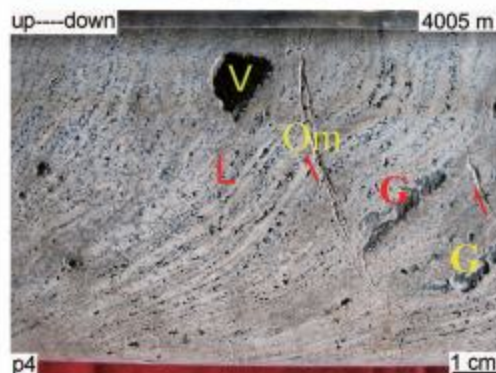
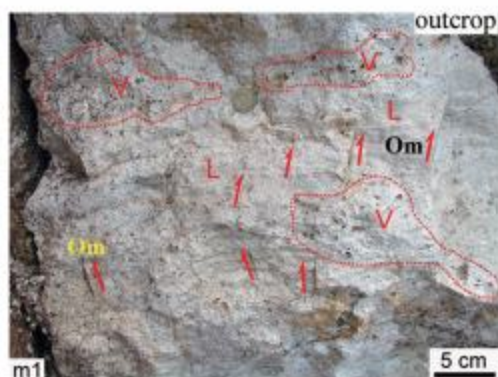
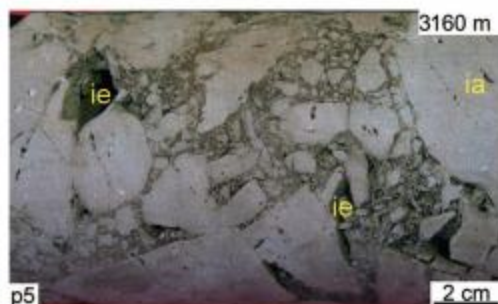
Textural evidence shows that vesicles and other primary textures of lava undergo similar preservation in both outcrop (Figure 4p1, m1) and deeply buried samples (Figure 4p2–p4, m2). The sizes, shapes, and orientation of the vesicles are well preserved in their primary state for the two groups of samples because the vesicles are actually interlaminated with lava flow bands. In contrast, deeply buried pyroclastics (Figure 4d2–d4) are much more densely compacted than the shallow samples (Figures 4d1, 9C, D).

PROXIMAL FACIES ASSOCIATION

Similar to facies delineations in modern volcanos (Steward and McPhie, 2006), the Lower Cretaceous volcanoes buried in the SB can also be described by three facies associations of proximal, medial, and distal in terms of distance from edifice. The proximal is characterized by a lava-rich dome and within a radius of 1 to 2 km (0.62 to 1.2 mi) in the volcanic center. The medial is a wedge-shaped volcanogenic zone around the proximal and with a general width of 1 to 3 km (0.62 to 1.9 mi). The distal is normally a kind of pinching-out pyroclastic deposit with unidirectional length from 1 km (0.62 mi) to more than 5 km (3.1 mi). They can be recognized in outcrops, core sections, well logs, and seismic data (Guo et al. 2006; Tang et al., 2008; Wu et al., 2010). In

Figure 4.

Representative volcanic facies associations corresponding to Table 3: proximal (p1–p7, labeled on the lower left corner), medial (m1–m5), and distal (d1–d4) facies associations, Lower Cretaceous Yingcheng Formation (K_1y) of the Songliao Basin. Photos of p1, m1, and d1 were taken from the stratotype outcrop and others from borehole cores in the Xujiaweizi graben and Changling graben (cf. Figure 1). Meters on the upper right corner are the depth of burial. The rocks include rhyolite (p1–p4, p7, m1–m3), in situ breccia with concrete-like texture (p5), hydrothermal jigsaw-fit breccia (p6), welded ignimbrite with flowing band (m4, m5), lapilli or lapilli tuff (d1–d3), and tuffaceous conglomerate (d4). V = vesicle or vesicle group, G = gas pipe, L = lava flow laminae, H = hydrothermal deposits of iron-rich silica, Fe = alteration byproducts rich in iron, ie and ia = inter- and intra-grain pore, uc = unfilled crack, pg = pore in groundmass, pc = pore in clast. Or = orthoclase, note the tail behind Or and its envelope twin in m5. Bold yellow arrow in m5 indicates lava flow direction. Red arrows indicate fractures of



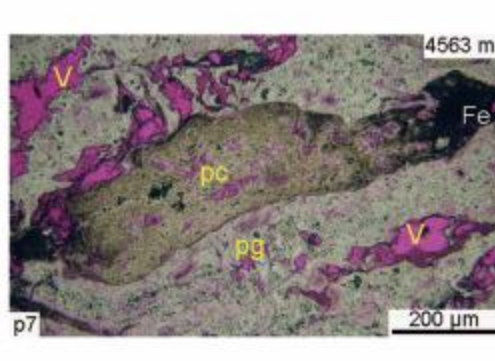
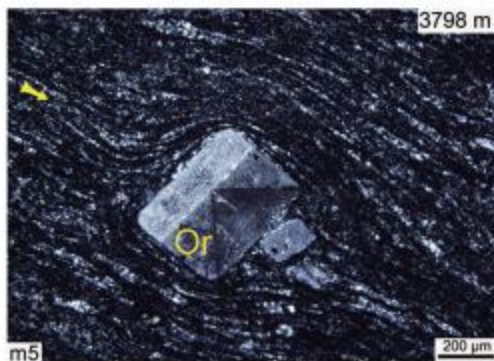
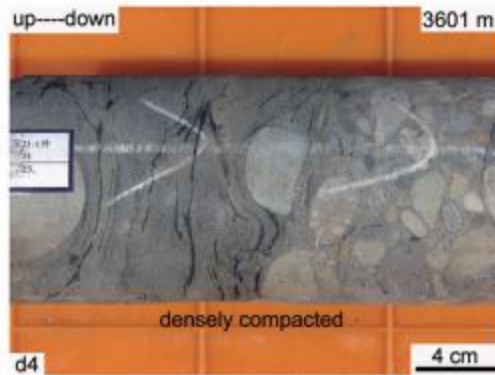
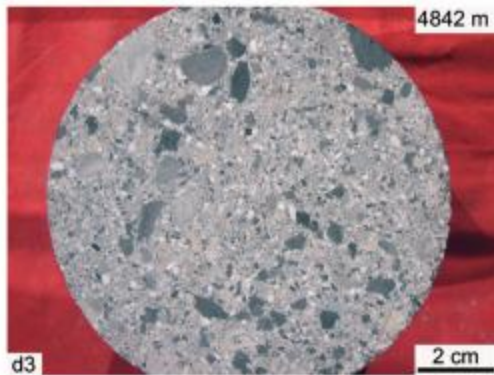
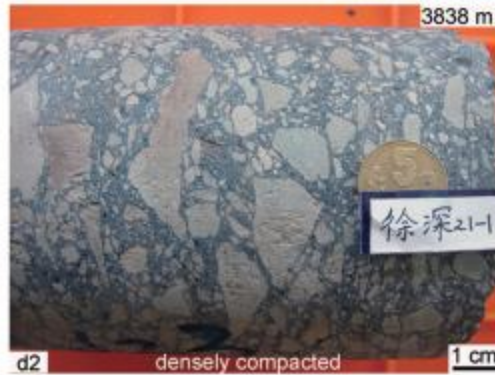
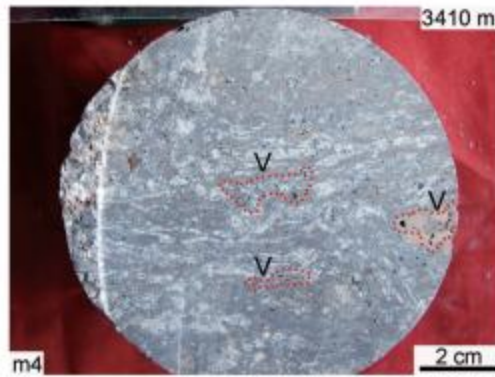
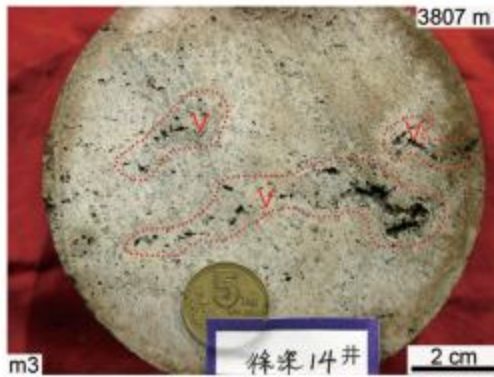


Figure 4. Continued. different direction that may result from cooling (Cf), flaty joint (Fj), opening mode (Om), or fault (F). Interflow laminar vesicles are widespread in p1–p6 and m1–m3. On the inner wall of the vesicle-lined quartz crystals (p2). Geopetal structure of flowing molten lava can be seen in p4 where bottom of the vesicle (V) is flat and parallel to the lava flow laminae, and the top is convex.

Table 3. Reservoir Performance of Proximal, Medial, and Distal Volcanic Facies Associations of the Songliao Basin*

Parameters	Proximal Facies Association	Medial Facies Association	Distal Facies Association
Chemical composition	Rhyolitic, andesitic, and basaltic	Rhyolitic, andesitic, and basaltic	Felsic to mafic; volcanic to nonvolcanic
Typical lithologic association	In situ breccias of various origins, lava, hyaloclastite, and welded ignimbrite	Lava, ignimbrite, tuff, and tuffite	Tuff, tuffite, tuffaceous epiclastics, and coal
Structural and textural diagnostics	Jigsaw-fit and concrete-like structures, vesicle/gas pipe, columnar joint, deformed lava flow structures	Fluidal clast, vesicle, and lava flow structures; stratification of pyroclastics with various bedding	Beds: stratification, massive to graded, and clast- to matrix-supported; Clasts: angular to rounded, volcanic to nonvolcanic
Interpretation of facies unit or emplacement environment	Caldera, massive coherent lava, fallout, domes and collapse, and conduit assemblage including vent, shallow intrusives, and crypto-explosives†	Effusive massive coherent lava; explosive pyroclastic flow, surge, and fallout	Primary to reworked; high- to low-energy environments including gravity flow, alluvial fan, fluvial, and swamp; ash fall in lake
Unidirectional length × thickness**	1 to 2 km × 200 to >500 m (ca. 1–2 km in center)	1 to 3 km × 100 to 300 m (ca. 2–5 km from center)	1 to >5 km × 10 to 150 m (ca. 3 to more than 10 km from center)
Typical shape of volcanostratigraphy** (cf. Figure 10)	Top: doming; Bottom: tree rootlike down to deep; Profile: volcanic high	Top: wedged; Bottom: flat, but pre-eruption topography controlled; Profile: volcanic slope	Top: planar or evenly wedged; Bottom: flat, but pre-eruption topographic controlled; Profile: volcanic edge
Major types of reservoir pore spaces (see Figure 4)	Vesicle, amygdule, gas pipe, intra- and inter-grain pores of different kind, fracture and crack of different origin, interflow laminar vesicle, and drusy	Vesicle, amygdule, intra- and inter-grain pores of different kind, fracture and crack of tectonic origin, and interflow laminar vesicle	Intra- and inter-grain pores of different kind, fracture and crack of tectonic origin
Average porosity contribution§	Pores	Bulk: 7.7%; Aperture space as one: 62%	Bulk: 3.3%; Aperture space as one: 75%
Porosity (vol. %)	Fractures	Bulk: 4.7%; Aperture space as one: 38% Max. 22.0, min. 0.9, mode 5.0, mean 7.1, number 413	Bulk: 1.1%; Aperture space as one: 25% Max. 14, min. 0.2, mode 3.0, mean 4.3, number 73
Permeability (10 ⁻³ μm ²)		Max. 95.0, min. 0.003, mode 0.1, mean 0.7, number 413	Max. 4.7, min. 0.002, mode 0.02, mean 0.2, number 73
Initial lithification style#	Solidified by cooling and/or crystallizing	Consolidated by cooling coupled with compaction	Consolidated by compaction
Overburden pressure resistance	Strong, as a result of the high proportion of rigid rocks such as lava and welded ignimbrite	In the middle	Relatively low
Primary pore spaces**	Abundant, partly a result of high primary volatile release	In the middle	Relatively low
Secondary processes**	Frequently occurred because of active geothermal fluid and tectonic weakness in the volcanic center	In the middle	Relatively low

See text for explanation

Tectonic brecciation following volcanism	Strong, because of the tectonic weakness coupled with frequent intrusions	In the middle	Relatively low
Heterogeneity	Strong, because of the sharp changes in lithology and fracture associations	In the middle	Relatively low
Representative appearance shown in Figure 4	From p1 to p7	From m1 to m5	From d1 to d4

*Statistical results based on the work of Wang et al. (2007c), with measurement of exposed volcanoes on southeast margin of the Songliao Basin and buried volcanoes revealed by borehole and three-dimensional seismic data in the Xujiawei graben (Figure 1).

†Concrete-like or piled-up structure was frequently observed near the volcanic center, in a special kind of in situ breccia that looks like a pile of concrete (cf. Figure 4p5). It is composed of angular fragments of different sizes that are loosely cemented together in most cases.

‡Crypto-explosive facies, as shown in Figure 4p6, indicate that underground explosions result in a series of in situ breccia and jigsaw-fit structure because of the high pressure of volatiles coupled with fluids following a major volcanic event. The time span between the two events of lava and subsequent fluid is in general within 1 Ma in the Songliao Basin (Wang et al., 2010).

§Based on image analysis, see text for further explanation. The average contribution of pore to bulk porosity is more than 60% for all the three facies associations. It is in contrast with deeply buried, tight sandstones, such as Cozzette Sandstone, where the maximum burial depth is about 4000 m (13,123 ft), and the porosity is primarily fracture related (Hooker et al., 2009).

||Data in Tables 1 and 2 were processed based on three facies associations (proximal, medial, and distal).

#Determined with thin section (e.g., Figures 4m5, 9) and referenced to Gao et al. (2007).

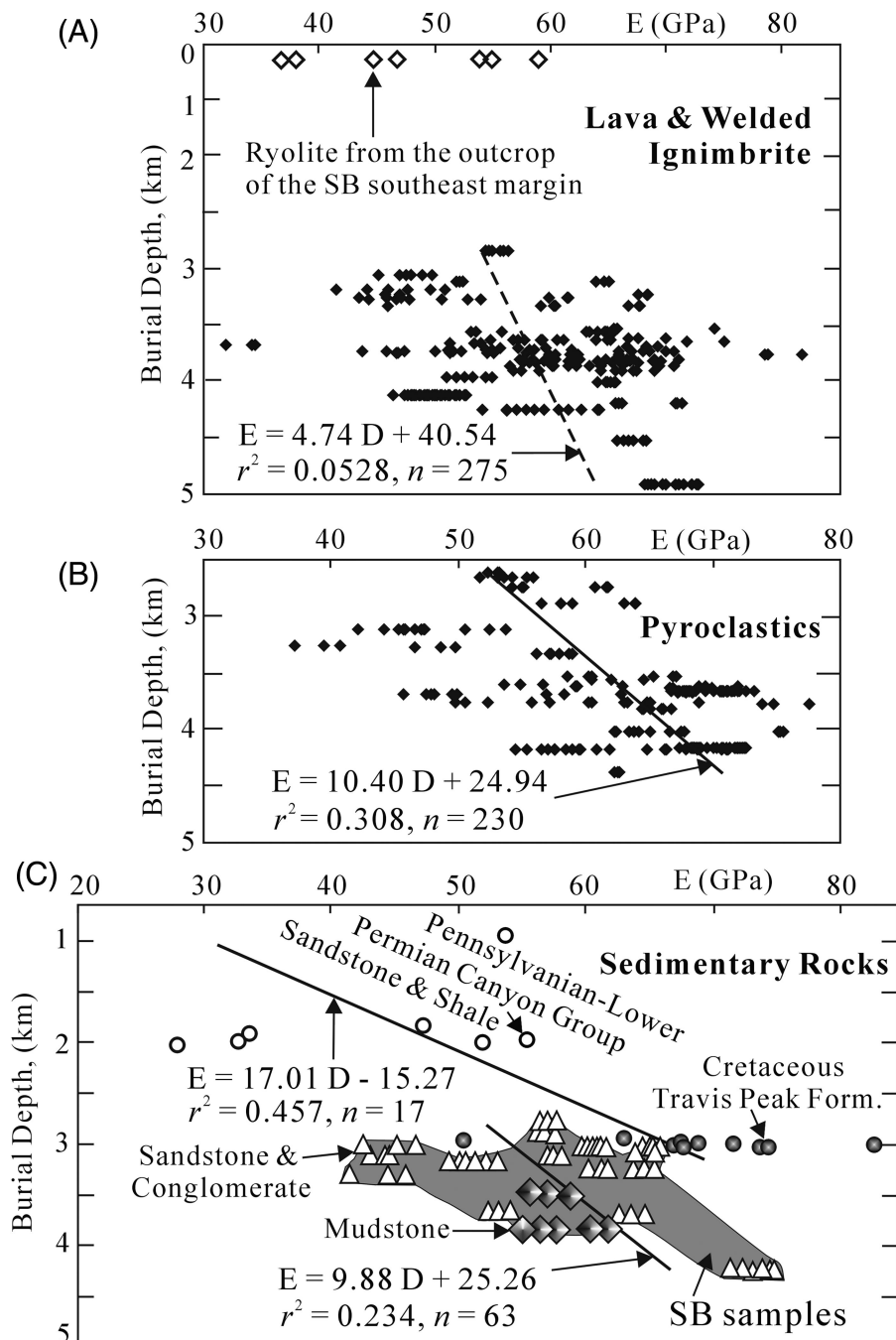
**Note: Features such as edifice appearance, amygdale development, and deuteric diagenesis may be different from rhyolite, andesite to basalt in the Songliao Basin (e.g., Huang et al., 2010; Liu et al., 2010). Because felsic volcanics are predominant, as described in Figure 3, rhyolitic and dacitic volcanic complexes are mainly described by this table.

Table 3, three facies associations were delineated by 17 key parameters as proximal, medial, and distal. Lithologic association, structure, texture, and volcanostratigraphic profile are the key criteria for diagnosing proximity to a volcanic conduit (see Figures 4, 10, 11). Proximal facies association is the most important control for effective volcanic reservoirs. It provides the most favorable conditions for effective volcanic-rock hydrocarbon reservoirs because of its optimal primary and secondary porosity and advantageous preservation. Hydrocarbon exploration in the volcanic rocks in the SB shows that the most productive areas are in buried volcanic highs situated in the centers of paleovolcanoes (Table 5).

Primary Porosity

The origin of most primary volcanic reservoir porosity in order of importance is (1) vesicles and gas pipes, (2) inter- and intra-grain spaces (pores between and within clasts, shards, and crystals), (3) interflow laminar voids, and (4) cooling fractures (Figure 4). These pore spaces may coexist with one another. They can also be affected by diagenesis and sealed by cements (Laubach, 2003). From the center to edge of the volcanic edifices, the size, density, style, and arrangement of porosity changes significantly. Comparing the proximal (Figure 4p1–p4) and the medial facies (Figure 4m1–m4), individual vesicles and gas pipes are obviously larger and more abundant in the central part of the volcanoes. In situ breccias of various kinds were well preserved in the volcanic vents, which provide abundant inter- or intra-grain pore space (Figure 4p5–p7). Criteria for recognizing major types of breccia are described in Table 3 and Figure 4. Lava flow structures are more prevalent near volcanic centers, and those structures are associated with numerous interflow laminar voids in the volcanic rocks (Figure 4p4). Cooling fractures (Figure 4p1) are frequently common in the proximal facies, especially for those lava rocks with columnar joints. In contrast, rhyolitic flow structures in the medial facies are more evenly spaced and have smaller vesicles (Figure 4m1, m2). Far from volcanic centers, in the distal facies association, primary pore spaces such as vesicles, gas pipes, or cooling fractures are absent (Figure 4d1–d4). The mean porosity

Figure 5. Young's modulus (E) versus burial depth (D) for the interbedded volcanic (A), pyroclastic (B), and sedimentary (C) rocks collected from 2600 to 5000 m (8530 to 16,404 ft) in the Songliao Basin (SB). Notes: (1) Seven outcrops of rhyolite show values from 37.2 to 55.9 GPa that drop within the range of deep samples (A). (2) For comparison with the SB sedimentary rocks, 7 Canyon Group samples from Sonora Gas Field, Texas (black circle) of Olson et al. (2009) and 10 of Travis Peak Formation in east Texas (grey dot) of Laubach et al. (2009) were plotted together in the upper part of c. The result as a whole shows depth-dependent features similar to those shown in the SB (shaded), although with a wider range.



in proximal, medial, and distal facies association is 7.1%, 5.9%, and 4.3%, respectively (Table 3).

Secondary Porosity

The predominant secondary pores are, in order of abundance, (1) faults and opening-mode (joint) fractures (probable tectonic origin) (Figure 4p1, p4), (2) pores formed by dissolution or alteration

(Figure 4p7), and (3) pores formed by hydrothermal breccia (Figure 4p6). In addition, recrystallization of volcanic glass may increase local pore space (Liu et al., 2010; Rowe et al., 2012). Fractures can be frequently observed in the volcanic complexes, especially close to fault zones or porphyritic dikes (Sun et al., 2007; Zheng et al., 2007). They mainly include opening-mode, cross joint, and longitudinal joints (Figure 4p1, m1) as classified by Pollard and Aydin

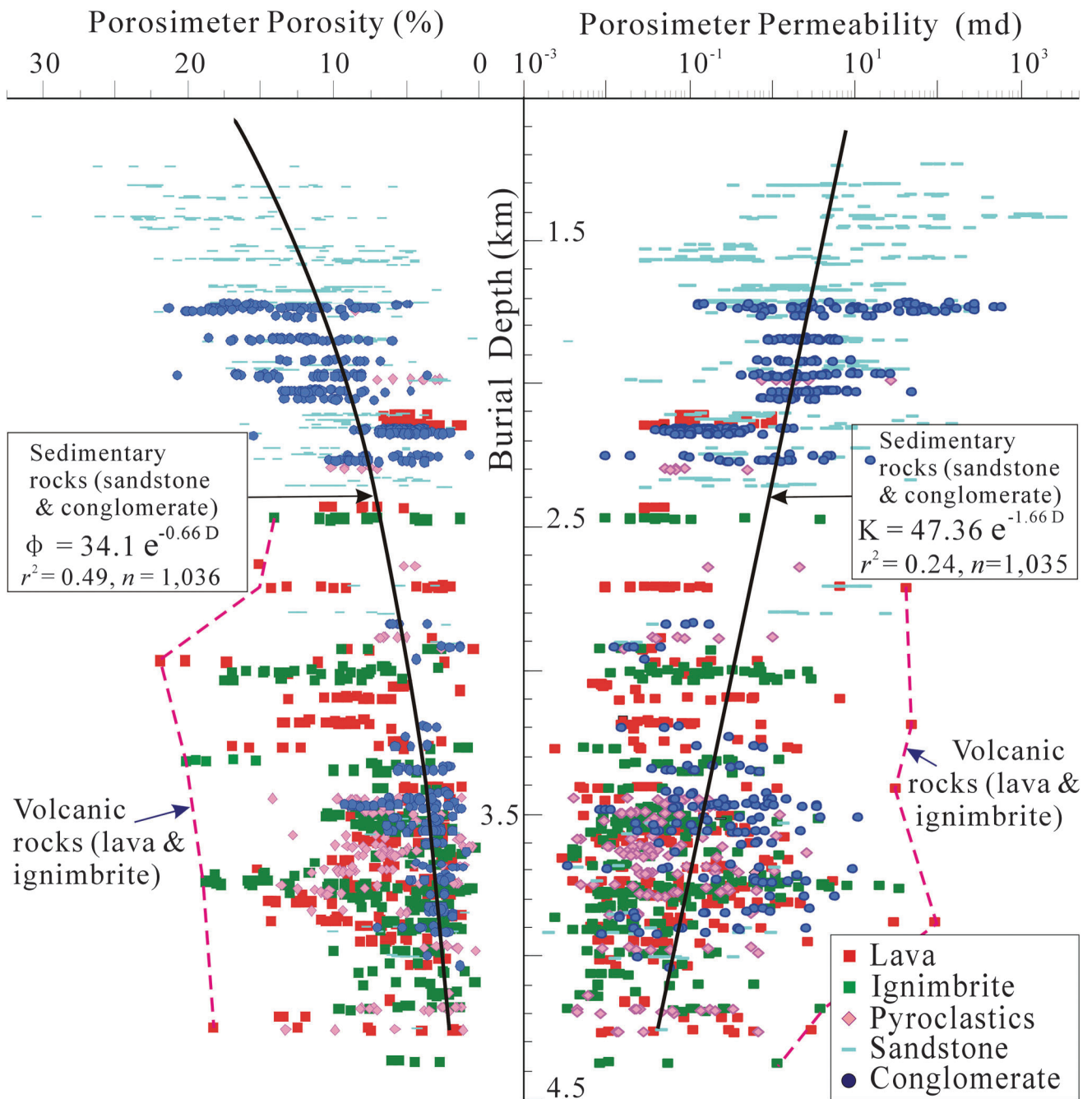


Figure 6. Trends in porosity (Φ) and permeability (K) versus burial depth (D) for volcanogenic rocks (lava, welded ignimbrites, and pyroclastics) and sedimentary rocks (sandstone and conglomerate). With increasing burial depth of about 3000 m (9843 ft), both porosity and permeability of the lava and welded ignimbrite become distinctly higher than those of the sedimentary rocks. Data correspond to Table 1.

(1988). With trace lengths from several millimeters to tens of meters, the fractures play major roles in connecting individual pore spaces (Figure 4p1, p4, m1, m2). Mapping of volcanic edifices shows that major craters are generally connected by transtensional or transpressional fault systems (Figure 10A; Wang et al.,

2007c). The contribution of recrystallization to pore development can be observed in the banded interflow laminae, in which lava flow structures are composed of interbedded layered pores and lava at millimeter scales (Figure 4p4, m2, m5). Pores and fractures are also affected by cement precipitation that reduces

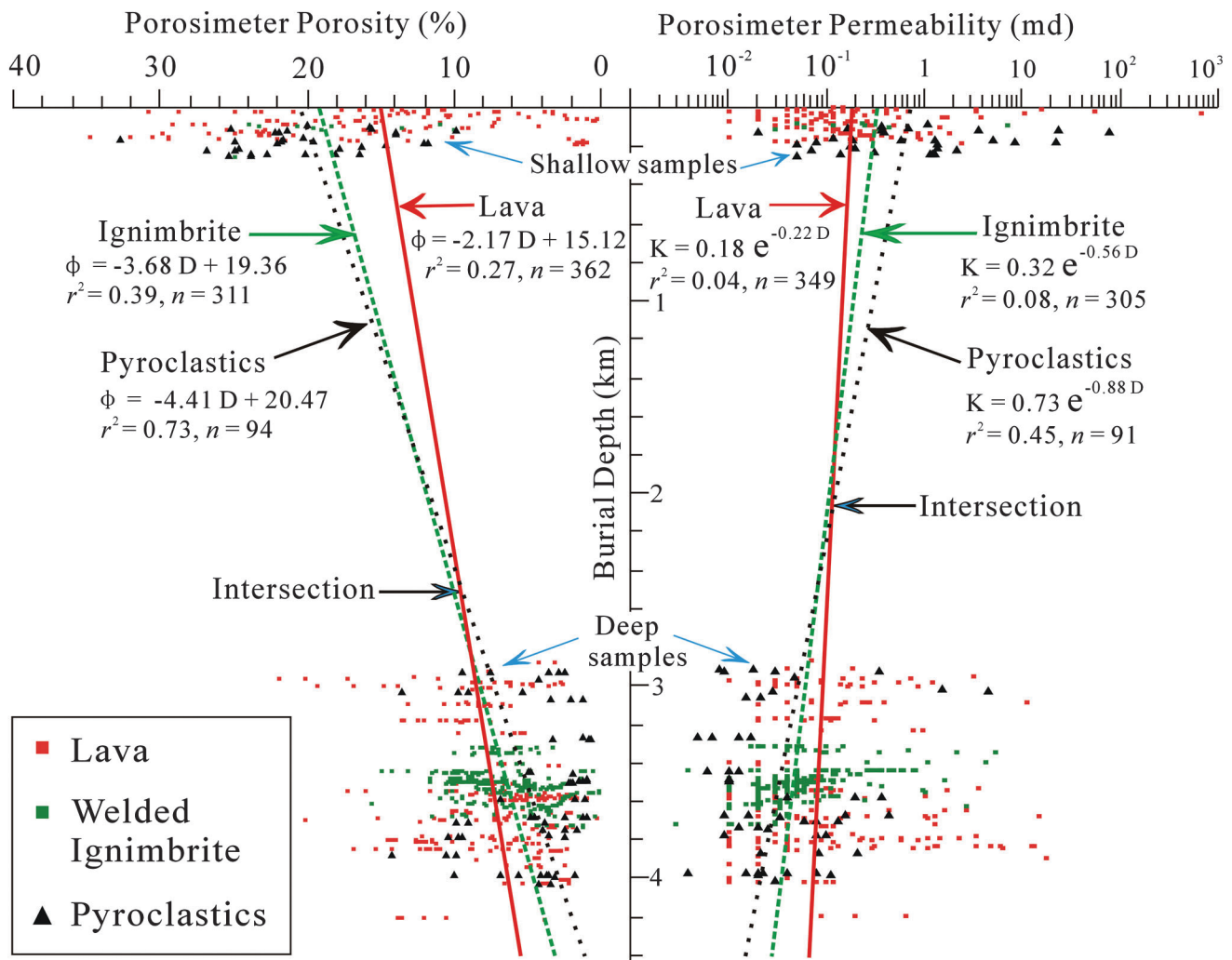


Figure 7. Trends in porosity and permeability versus burial depth among lava, welded ignimbrites, and pyroclastics. For burial depths shallower than 2000 m (6562 ft), both porosity and permeability are in the order of lava < welded ignimbrite < pyroclastic rocks, whereas below a depth of approximately 3000 m (9843 ft), they change to a reversed order, that is, lava > welded ignimbrite > pyroclastic rocks. Data correspond to Table 2.

porosity and especially permeability, as described by Philip et al. (2005). Fracture-filling phenomena are more frequently observed near a volcanic center. For example, hydrothermal breccias are often cemented with red iron-rich silica deposits (Figure 4p6), which are commonly recognized within 1 km (0.62 mi) from the central part of a paleovolcano. Precipitation and dissolution often coexist following volcanic events (Wang et al., 2010). Interaction between fracturing and filling can create new pore space in both clasts and groundmass in spite of simultaneous precipitation (Figure 4p6, 7). Although quartz and iron oxide deposits are commonly associated with the fractures

and pores mentioned previously, some portion of unfilled spaces generally remain as open-fracture pores, and others are incompletely filled pores (Figure 4p5, p6). The process of fracturing and filling is similar to the evolution of crack-seal texture described in crack sandstones (Laubach and Ward, 2006; Olson et al., 2009).

Preservation of Reservoir

An increase in induration and stiffness caused by overburden pressure is a major factor that reduces porosity and permeability of rocks (Figure 6). Thus,

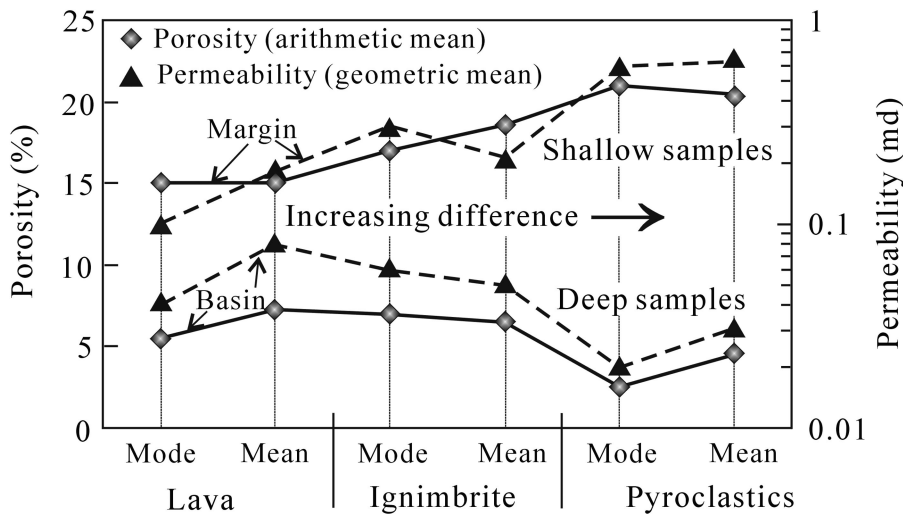


Figure 8. Overburden pressure influence on different volcanogenic rock types. Note that (1) shallow samples (margin) show significantly higher porosity and permeability than the corresponding deep (basin) samples for all of the rocks. (2) Differences between shallow and deep samples significantly increase through lava, ignimbrite to pyroclastics, indicating that reservoir parameters for lava change the least; whereas, pyroclastics change the most from shallow to deep. Data correspond to Table 2 and Figure 7.

resistance to overburden pressure depends on rock type, which influences porosity preservation. Unlike pyroclastic and sedimentary rocks, lavas show less change of their Young's modulus with burial depth (Figure 5), suggesting reduced sensitivity to overburden pressure ($r^2 = 0.05$ for the regression). The effect on Young's modulus from overburden pressure is greater for pyroclastic and sedimentary rocks ($r^2 = 0.2-0.5$). Lavas also show slower declining porosity and permeability versus depth (Figures 6, 7). The proximal facies association is mainly composed of lavas and other rigid rocks, including welded ignimbrites, hyaloclastites, and in situ breccias of various origins (see Figure 4 and Table 3). They mostly facilitate the preservation of primary porosity (cf. Figure 4p1-p4). In contrast, the distal facies association is predominantly composed of pyroclastic rocks, tuff, and tuffite (Figure 4d1-d4), which were initially consolidated by compaction (Table 3) and show faster porosity and permeability loss when deeply buried (see Figure 7).

DISCUSSION

Diagenetic Details of the Volcanogenic Successions

Both the volcanogenic and the interbedded sedimentary rocks suffered diagenesis that mainly includes

compaction, cementation, and alteration, as well as fracturing and infilling (Table 4). But they reacted differently to these diagenetic events. Compaction seems to have little influence on lava and ignimbrite because shallow and deeper samples show similar textures (Figures 4p1-p4, 9A, B) and comparable values of Young's modulus (Figure 5A). In contrast, pyroclastic and sedimentary rocks show tightly compacted and cemented grain contacts for the deep samples (Figure 9D, F). Fragments in clastics or phenocrysts in lavas show similar overgrowths of quartz and in minor cases feldspar, replacement of feldspar by sericite, and dissolution of feldspar or lithics from secondary pores (Figure 9E, F). The most significant difference of diagenesis occurred in the groundmass of the rocks, which show increasing cementation intensity from lavas to pyroclastics to sediments (Table 4). The groundmass shows insignificant change from shallow to deeper rhyolites (Figure 9A, B, E), both showing the original state of lava flow structures and crystallized features (Figure 4m5). The primary stiff groundmass may preserve contemporaneously formed, string-interbedded vesicle clusters (Figure 4p4, m2). The matrix of the pyroclastics is composed of fine volcanic ash that may partly change into clay minerals but is seldom replaced by quartz or calcite (Table 4). However, interbedded sandstones of mainly lithic arkose and feldspathic litharenite have minus cement porosity around 10% to 15%. Considering the complex composition, intergrain spaces in the sandstones could

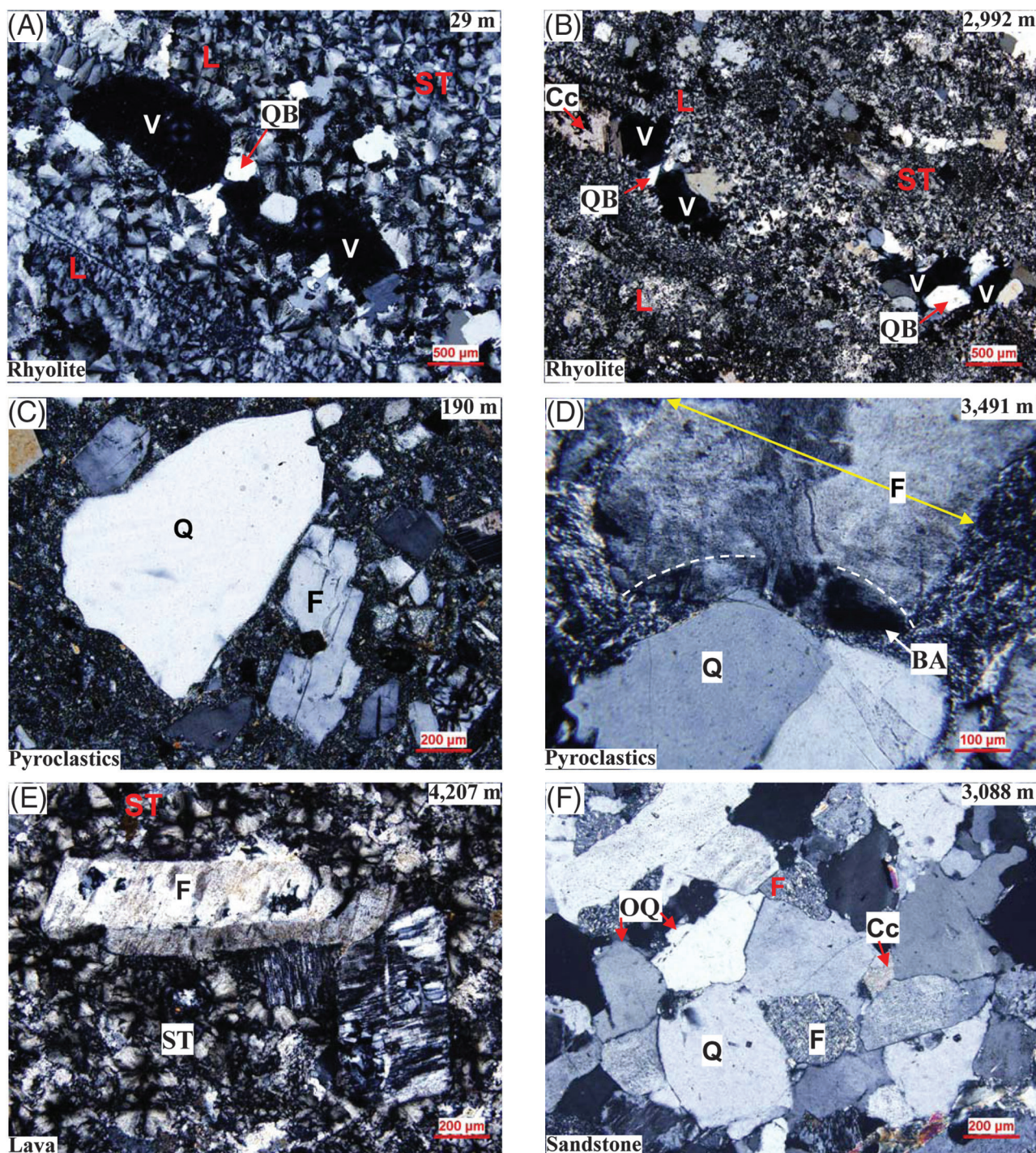


Figure 9. Polarized light microscope images show diagenesis versus burial depth among lava, pyroclastics, and sandstone samples. Note that (1) rhyolite both shallow (A) and deep (B) is similar in groundmass of spherulitic texture (ST), lava flow laminae (L), elongated vesicles (V), and quartz cement bridges (QB) in pores, but the deep samples (B) show more complicated vesicle infilling patterns both in style and composition. (2) Shallow pyroclastics (C) are loosely compacted with point contact grains; whereas, the deep samples (D) have convex contacts of grains and bent crystal axes (BA) of feldspar (F), likely caused by compaction. (3) Both deep lava (E) and sandstone (F) are similar in feldspar grain alteration (F = dirty surface with clay minerals), but their groundmasses are quite different. Spherulitic textures (ST) of the lava (E) are well preserved, showing little change of groundmass from the shallow samples (A). In contrast, the sandstone (F) is densely cemented by overgrowth quartz (OQ) and intergrain calcite (Cc). Sample burial depths (upper right corner) are in meters.

Table 4. Comparison of Diagenesis and Porosity versus Buried Depth: Among Lava, Pyroclastics, and Sedimentary Rocks, and Between Shallow and Deep Samples

	Rhyolite Shallow versus Deep		Pyroclastic Rocks Shallow versus Deep		Sandstone/Conglomerate
Burial depth (m)	25–50, n = 8	3061–4275, n = 10	154–202, n = 8	3187–3705, n = 10	3072–3088 m, n = 12
Fragment or phenocryst	Q ₃₀ F ₅₀ *, IV ≤ 12% (0.4–4.0)/1.2	Q ₄₅ F ₅₅ , IV ≤ 12% (0.4–3.0)/1.0	Q ₅₃ F ₂₄ R ₂₀ O ₁ , TV 35% (0.02–1.6)/0.3	Q ₂₉ F ₃₄ R ₃₇ , TV 70% (0.1–16)/1.1	Q ₄₀ F ₂₂ R ₃₅ O ₃ , TV 87% (0.21–3.1)/0.6
Grain size (mm) (min–max)/mean	Floating in groundmass	Floating in groundmass	Point contact or floating in groundmass	Straight and convex	Convex dominant
Grain contact relationship					
Primary groundmass and volume percent	Equivalent Q and F cryptocrystalline, ≥ 75%	Equivalent Q and F cryptocrystalline, ≥ 75%	Volcanic ash, 41%	Volcanic ash, 21%	Not preserved
Quartz cement or crack-infill	Quartz crack-infill, common	Quartz crack-infill, more common	Non	Quartz cement, 1.0%	Quartz cement, 9.3%
Calcite cement or crack-infill	Calcite crack-infill, common	Calcite crack-infill, more common	Non	Calcite cement, 1.5%	Calcite cement, 3.7%
Other cement or crack-infill	Zeolite, common	Zeolite, more common	Secondary clay mineral [†] 24%	Secondary clay minerals 6.5%	Non
Unfilled primary porosity on thin section	Vesicle, ±5%	Vesicle, ±4%	Non	Non	Non
Infilling mineral inside primary pores	Q, ±8%	Q + C + S + T*, ±9%	Non	Non	Non
Secondary porosity on thin section	Pores of intermicrocrystallite, 2.6%	Pores of intermicrocrystallite and grain dissolution, 3.2%	Pores of inter-clay mineral and grain dissolution, 3.0%	Pores of inter-clay mineral and grain/matrix dissolution 3.1%	Pores of grain/matrix dissolution, 3.4%
Porosimeter porosity	14%	9.1%	15%	8.0%	8.1%
Porosimeter permeability (md)	0.20	0.10	0.55	0.07	0.10

*TV = total volume percent; Q = quartz; F = feldspar; R = rock fragment; O = other fragments including biotite, muscovite, zircon, and epidote; S = siderite; C = calcite; T = thomsonite. The subscripts in Q₅₃F₂₄R₂₀O₁ represent percentage of the fragment when grains are considered as one.

[†]Secondary clay minerals are predominantly illite and may result from alteration of volcanic ash.

[‡]Intermicrocrystalline pores observed under both optical and electron microscope were likely formed by devitrification after magma cooling (Liu et al., 2010).

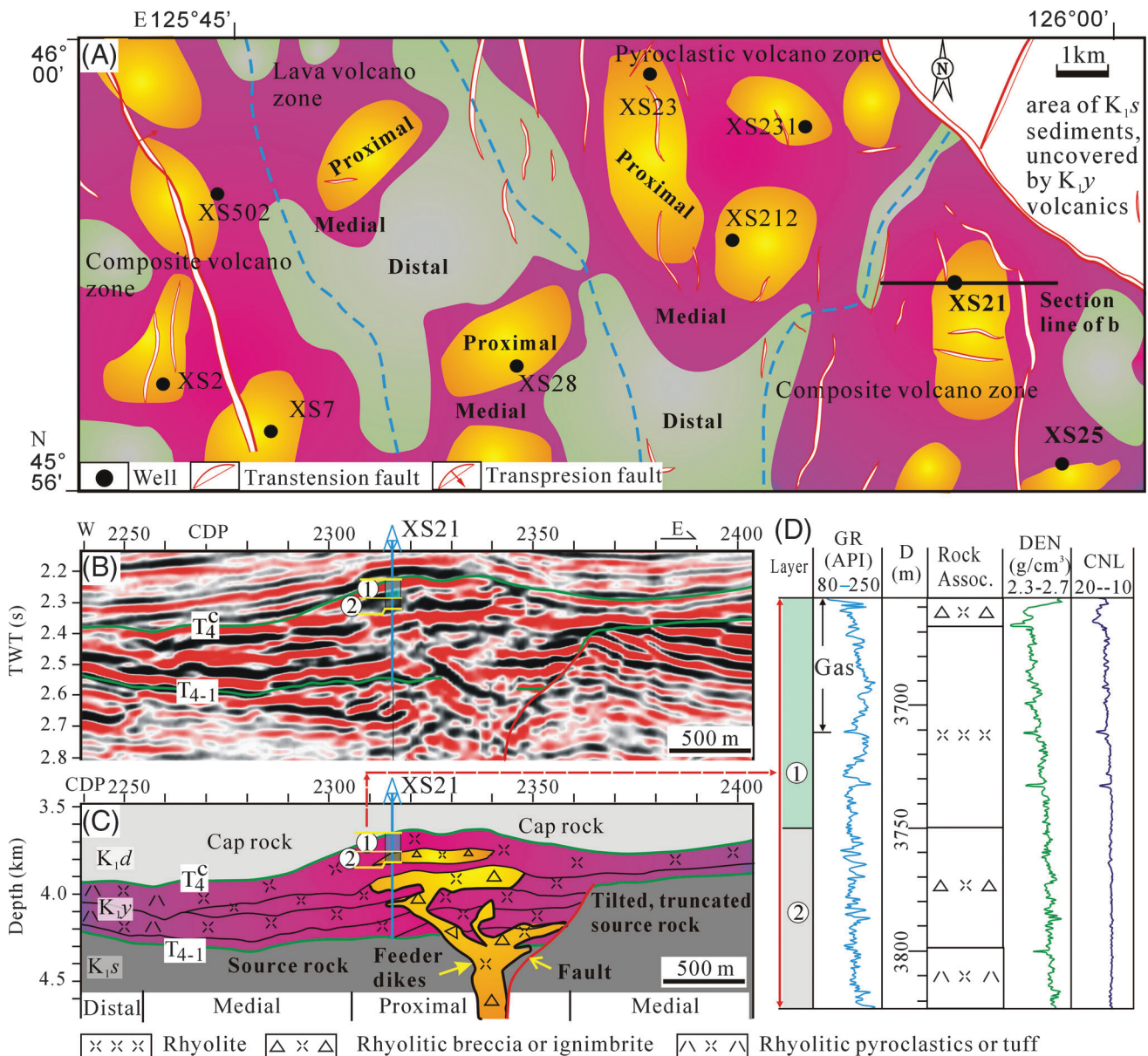


Figure 10. Representative volcanic reservoirs in the Songliao Basin. (A) Plan view of buried volcanic complexes of the Yingcheng Formation (K_{1y}), with facies distribution and fault patterns (area, see Figure 1). Bright yellow, pink, and gray colors indicate proximal, medial, and distal facies. (B) Seismic profile and well. (C) Interpreted section showing volcanic facies associations and petroleum system. (D) Well logs, lithologic section, and gas accumulation. Note that (1) seismic reflectors T_{4-1} and T_4^c and formation symbols of K_{1s} , K_{1y} , and K_{1d} are the same as in Figure 2. (2) Interpretations of volcanic facies are based on mean dip angles of 3-D seismic data, which are constrained by boreholes and well logs using methods described by Tang et al. (2007, 2008) and Wang et al. (2007c). (3) Compare to Figure 11, volcanic facies may be more detailed because non-cone-shaped volcanos can be included in (A).

have been originally occupied by clay. However, now they are largely cemented by quartz (7% to 14%) and calcite (1% to 4%), suggesting a strong cementation process (Figure 9F). It should be noted that the mass ratio between groundmass and grains is entirely different for the volcanics and clastics. The groundmass

volume of lavas is $\geq 75\%$ (phenocryst $\leq 12\%$, vesicles and infillings $\sim 13\%$), whereas that of sedimentary rocks is 13% (fragments $\sim 87\%$) (Table 4). Preservation of porosity in volcanic rocks largely depends on primary pore space associated with this groundmass (Figure 9A, B).

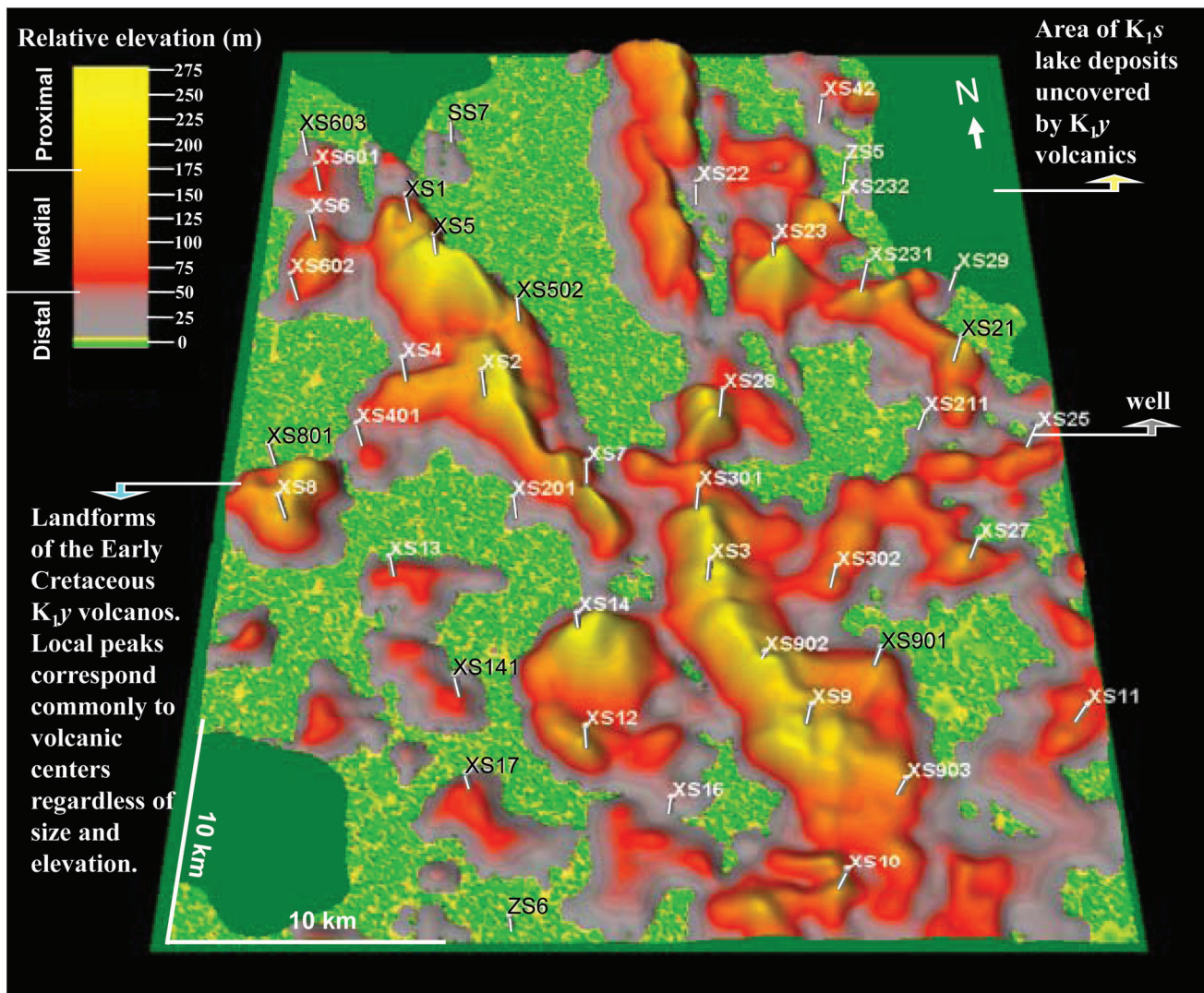


Figure 11. Three-dimensional map of buried volcanos in the Xujiaweizi graben (XG in Figure 1). Note: The proximal (near vent), medial, and distal facies associations are transitional and interfingering with each other. There are commonly not clear boundaries between them. In plan view, they approximately cover ~20%, 30%–50%, and 30%–50% of the area of a volcanogenic region, respectively. Some non-cone-shaped volcanos may be shown as distal in this map (see text for detail).

Figure 6 shows that porosity and permeability are inversely proportional to burial depth for the sandstones and conglomerates. Both parameters decline quickly in the upper part (likely due to compaction) and then decrease more slowly (diagenetic influence). Between 2000 and 3000 m (6562 and 9843 ft), porosities of both volcanic and sedimentary rocks nearly match. Below 3000 m (9843 ft), lava and ignimbrite show higher porosity than the sedimentary rocks, probably because of groundmass preservation of the primary porosity in lavas. The permeability curve shows a similar trend.

Similar to the sedimentary rocks but unlike lava rocks, pyroclastic rocks were initially consolidated by compaction. Increasing overburden pressure may densely compact pyroclastic rocks as shown in Figures 4d2, d3, 9D. However, sedimentary rocks, especially sandstones, are undoubtedly the best reservoir rocks worldwide. Pyroclastic rocks in the SB show textures similar to sandstone and conglomerate (see Figure 4d1–d4). Their poor reservoir capacity can be explained by the intersections in Figure 7. Porosity of pyroclastic rocks is better than lavas above the intersection depth of 2500 m (8202 ft).

Table 5. Volcanic Reservoir Exploration Examples in the Xujiaweizi Graben. Wells Correspond to Figure 11, except SS2 (See Figure 1)

Well No. /Bottom Depth (m)	Reservoir Rocks (Depths)/ Thickness (m)	Porosity (%)/ Permeability (md)	Volcanic Facies	Gas/Water Production (m ³ /day)
SS2/3053	Lava (2923–2995)/72	17.8/5.64	Proxim	307,890/0
XS42/4015	Pyroclastics (3702–3711)/9	11.5/0.10	Distal	461/0
SS7/3889	Pyroclastics (3698–3705)/7	4.4/0.24	Distal	8290/0
XS603/3767	Igimbrite (3514–3521)/7	10.3/0.13	Medial	260,357/0
ZS5/4507	Pyroclastics (3544–3615)/71	4.5/0.07	Distal	34/5
XS601/3705	Igimbrite (3551–3558)/7	9.6/12.21*	Proxim	232,098/0
XS1/4548	Igimbrite (3592–3624)/32	8.1/0.26	Proxim	530,057/0
XS22/5320	Igimbrite (4031–4038)/7	7.1/0.3*	Distal	4467/39
XS232/4238	Igimbrite (3862–3870)/8	5.7/0.66	Medial	597/87
XS6/4060	Igimbrite (3629–3637)/8	16.9/13.6	Proxim	105,689/125
XS5/4057	Igimbrite (3611–3629)/18	3.6/0.04	Proxim	121,982/0
XS23/4414	Lava (3909–3943)/34	10/4.36*	Proxim	188,244/0
XS602/4141	Sand. and Cong. (3657–3686)/29	5.9/0.35*	Medial	9838/0
XS231/4064	Lava (3732–3745)/13	3.7/0.03	Proxim	49,156/0
XS29/3687	Igimbrite (3579–3586)/7	6.5/0.15	Distal	15,625/0
XS502/4361	Igimbrite(4119–4127)/8	1.9/0.01*	Medial	Dry
XS4/4052	Pyroclastics (3873–3881)/8	4.9/0.4*	Medial	77,315/113
XS21/4273	Lava (3674–3703)/29	10.1/2.76	Proxim	206,446/0
XS2/4447	Lava (4076–4083)/7	8.2/0.32*	Proxim	23,000/20
XS28/4427	Lava (4167–4176)/9	13.8/0.65	Proxim	105,876/0
XS211/4291	Igimbrite (4094–4107)/13	5.7/1.08	Distal	9886/0
XS401/4546	Igimbrite (4182–4190)/8	9.4/0.23	Proxim	62,861/110
XS25/4483	Sand. and Cong. (3560–3570)/10	7.5/0.32	Medial	324/0
XS801/4110	Pyroclastics (3759–3766)/7	11.4/0.09	Medial	2981/65
XS7/4510	Igimbrite (3874–3880)/6	10.7/36.51*	Proxim	217,416/0
XS8/4228	Lava (3723–3735)/12	18.8/17.20	Proxim	226,234/0
XS201/4333	Lava (4038–4045)/7	8.4/0.07*	Distal	4692/101
XS301/4370	Lava (3943–3950)/7	8.8/4.63	Proxim	79,352/54
XS13/4450	Lava (4242- 4249)/7	10.5/0.03	Proxim	10,812/0
XS3/4763	Pyroclastics (3935–3944)/9	11.6/0.95*	Proxim	41,872/64
XS27/4180	Lava (3968–3976)/8	7.0/0.08	Proxim	102,063/0
XS302/4225	Igimbrite (3946–3968)/22	2.8/0.01*	Medial	Dry
XS14/4170	Lava (3788–3809)/21	14.5/2.25	Proxim	74,034/3
XS141/4242	Lava (3923- 4033)/110	9.6/0.08	Proxim	53,053/0
XS902/4275	Lava (3770–3779)/9	11.1/9.08*	Proxim	211,127/0
XS901/4100	Lava (3899–3912)/13	9.7/1.38	Proxim	148,036/0
XS12/3950	Igimbrite (3625–3642)/17	9.8/0.26*	Medial	51,749/0
XS9/4311	Lava (3592–3675)/83	7.7/17.10	Proxim	209,350/29
XS11/4095	Igimbrite (3632–3641)/9	7.1/0.17	Proxim	13,242/159
XS17/3980	Lava (3645–3652)/7	13.1/0.04	Medial	4510/0
XS16/4100	Pyroclastics (4004–4015)/11	1.8/0.01*	Distal	Dry
XS903/4085	Lava (3861–3893)/32	5.5/1.07	Medial	78,229/46
XS10/4197	Lava (3802–3812)/10	6.6/0.15	Proxim	19,361/69
ZS6/4117	Lava (3542–3706)/164	9.8/0.28	Distal	123/32

Note: Data are from well tests. Porosity and permeability are both porosimeter and logging (those with *). Volcanic facies correspond to Figure 11.

The permeability curve shows a similar trend in Figure 7, but with a shallower intersection at 2000 m (6562 ft), which suggests that permeability declines faster than porosity during burial and implies that permeability may be more sensitive to overlying pressure than porosity. These observations suggest that pyroclastic rocks, including tuff and tuffite in Figure 3, may be better reservoirs than lava and welded ignimbrite shallower than the intersection depth. The intersection depths may account for the fact that pyroclastic reservoirs have rarely been found in the SB because they are now generally deeper than 2500 m (8202 ft). Therefore, tuffaceous reservoirs could be better targets than lavas above the depth of about 2500 m (8202 ft) in the basin.

The Paleovolcano Volcanic Highs: Inheritance versus Variation

The explored volcanic highs formed during the Early Cretaceous underwent synrift block faulting followed by subsequent postrift subsidence in the SB (Wang et al., 2007a; Feng et al., 2010). The volcanic architectures likely changed during such a long time period, but little is known about these changes.

The buried volcanic edifices can be classified into two groups, cone-shaped and non-cone-shaped, according to their present topographic expression. The latter is much less common than the former, and it can still be identified by facies associations in core sections coupled with seismic data (Tang et al., 2007). These non-cone-shaped volcanoes could be original structures, but they are often also accompanied by widespread truncations (Wu et al., 2010), implying significant posterection erosion and reworking. However, most of the buried volcanoes appear as domes in profile (Figure 10C), and they show facies architectures very similar to those of modern examples (e.g., Steward and McPhie, 2006) or their counterparts exposed at the basin margin (Wang et al., 2007b). Based on these observations, we believe that most of the volcanoes have retained their original structures and lithological assemblages since the Early Cretaceous. This conclusion can to some extent be supported by exploration results showing that volcanic highs mostly correspond to proximal facies

associations (Figure 10). Two favorable factors have been identified for the formation of gas traps on volcanic highs. One factor is the well-developed reservoir spaces in proximal volcanic facies associations as listed in Table 3. The second factor is that structural highs represent favorable locations for gas migration and accumulation.

Controls on the Effective Volcanic Reservoirs

Effective reservoirs in this study are volcanic rocks containing proved gas and/or water. Exploration history of the SB during the last 15 yr indicates that effective reservoirs largely depend on porosity and permeability relative to their adjacent units. Fluids, either gas or water, tend to enter the rocks with better reservoir parameters regardless of whether their values are high or low, unless their porosity or permeability are below critical values of 3% or $0.01 \times 10^{-3} \mu\text{m}^2$, respectively. In the course of exploration, it is common to see that a unit with 5% porosity may become an effective reservoir if the porosities of the adjacent units are lower. Alternatively, a unit with 10% porosity may be dry if adjacent units show higher porosity. Thus, relative values of porosity and permeability are the controlling factors for effective volcanic reservoirs. This finding is significant because it explains that it is easier to find good reservoirs within large-scale volcanic architectures than to detect high-porosity reservoirs in other types of lithologies.

For a thick volcanogenic succession, reservoir behavior depends on the volume ratio between rocks having different styles of initial lithification. Higher percentages of lava and ignimbrite typically yield better reservoir parameters in the deep basin. In our case, the proximal facies associations are composed mainly of rigid rocks including lavas, welded ignimbrites, hyaloclastites, and in situ breccias of various origins (cf. Table 3 and Figure 4p1–p7). Primary pore spaces are best developed there, which may be a result of more volatile release closer to a volcanic crater (Sruoga and Rubinstein, 2007). Fracture-generating secondary processes occurred preferably in volcanic centers, which may be ascribed to tectonic weakness there. Combinations of primary, secondary, and preservation conditions created the effective volcanic

reservoirs that most frequently occurred in the proximal facies associations.

Exploration Examples for Volcanic Reservoirs

The first high-production volcanic gas well (SS2 in Table 5) was by chance drilled in 1994 in the SB. However, the cuttings of the spherulitic rhyolite were wrongly described as fine quartz sandstones. Two yr later, an interesting question was raised as how could such pure quartz sandstone with more than 90% quartz form in the graben during the synrift stage (Figure 2)? Thin-section work on the cuttings gave the answer: They are actually high silica lava. The volcanic reservoir has become a new kind of exploration area since then. However, wildcat success rate was very low (below 20%) during the first 10 yr for volcanic exploration because no one knew where to drill for this kind of reservoir. Most of the high-production wells such as XS1 and XS21 (shaded in Table 5) were drilled on local volcanic highs in the past 10 yr when volcanic centers have been considered favorable targets. To know the location of the paleovolcanoes, we need to map them both geologically and seismically. That involves three parts: (1) establishment of volcanic facies models based on sufficient outcrop observations as summarized in Table 3, (2) borehole description on vertical successions concerning lithology and volcanic facies similar to the style in Figure 10D, and (3) borehole-constrained interpretation of two-dimensional and three-dimensional seismic data as in Figure 10B, C.

Cone-shaped paleovolcanoes are common in the SB probably because of their high silica content. These volcanic landforms may be approximately reconstructed when a marker bed of lacustrine or swamp deposit under the volcanic successions is flattened by seismic data because this kind of marker bed may roughly represent certain pre-eruption paleoplanes. A widely distributed coal bedding (K_{1s}) under the volcanogenic succession (K_{1y}) has been used as the marker bed in Figure 11. Fault movements have been simultaneously shifted back accompanying the flattening operation. Local paleovolcanic highs correspond commonly to volcanic centers, the proximal facies associations in this case. Mean dip

angles of three-dimensional seismic data are also frequently used to map buried volcanos, which can delineate both cone-shaped and non-cone-shaped ones (Tang et al., 2007).

Hydrocarbon gases are predominantly found in the volcanic reservoirs (Table 5). This may attribute to the organic maturity and kerogen quality. Source rocks of the K_{1s} are interbedded black shale and coal (Figure 2). Total organic carbon for the shale (coal) is 0.5%–6% mean 1.59% (6%–80% mean 32.8%). Type-III kerogens are dominant with vitrinite reflectance ranging 1.27%–3.56%, average 2.38% (J. K. Li et al., 2006). Fault systems coupled with truncation surfaces shown in Figure 10B are likely the major paths for gas migrating into the volcanic reservoirs. A reasonable migration distance is inferred within several kilometers both laterally and vertically according to the association between reservoir and source rocks in Figure 10B, C.

CONCLUSIONS

In order to explain how to locate effective volcanic reservoirs, we summarize the main conclusions drawn from the previous sections as a strategic exploration guideline. (1) Lavas and welded ignimbrites show better porosity and permeability than pyroclastics and normal sedimentary rocks when exploration targets are located below 3000 m (9843 ft) in the SB, mainly due to differential burial diagenesis. (2) Proximal facies associations contain the highest portion of lavas and welded ignimbrites within a volcanic edifice; therefore, those reservoir properties are the best. (3) Volcanic highs are generally situated in the central parts of buried volcanoes because the original paleotopography is usually preserved. (4) Effective reservoirs are preferentially developed in those volcanic highs that show alternating associations of lithology and facies architecture because this can provide favorable combinations of reservoirs and seals. Composite volcanoes can frequently meet this criterion in the SB (Tang et al., 2007, 2008).

Thus, practical exploration procedures used to discover effective volcanic reservoirs in the SB include mapping of volcanic provinces within the basin, delineating different types of paleovolcanoes,

searching for and selecting composite paleovolcanoes by drilling on volcanic highs, and choosing reservoir units with the best porosity and permeability. Additionally, the reservoirs must be close to petroleum source rock, as shown in Figure 10. Three critical depths should be taken into account in the exploration process for petroleum in the SB. At burial depths shallower than 2000 m (6562 ft), sedimentary rocks (sandstones and conglomerates) are the preferred targets because of their higher porosity and permeability. Below 3000 m (9843 ft) depth, lavas and welded ignimbrites are the best reservoirs because of their strong resistance to overburden pressure. Between 2000 and 3000 m (6562 and 9843 ft), both sedimentary and volcanic rocks may be considered as target reservoirs. The reservoir performance of pyroclastic rocks is similar to that of sedimentary rocks with respect to porosity-depth relationships.

REFERENCES CITED

- Chen, Z. Y., H. Yan, J. S. Li, G. Zhang, Z. W. Zhang, and B. Z. Liu, 1999, Relationship between Tertiary volcanic rocks and hydrocarbons in the Liaohe Basin, People's Republic of China: *AAPG Bulletin*, v. 83, no. 6, p. 1004–1014.
- Einsele, G., 2000, *Sedimentary Basins*: Berlin, Heidelberg, New York, Springer-Verlag, 792 p.
- Feng, Z. Q., 2008, Volcanic rocks as prolific gas reservoir: a case study from the Qingshen gas field in the Songliao Basin, NE China: *Marine and Petroleum Geology*, v. 25, p. 416–432, doi:[10.1016/j.marpetgeo.2008.01.008](https://doi.org/10.1016/j.marpetgeo.2008.01.008).
- Feng, Z. Q., C. Z. Jia, X. N. Xie, S. Zhang, Z. H. Feng, and A. C. Timothy, 2010, Tectonostratigraphic units and stratigraphic sequences of the nonmarine Songliao Basin, northeast China: *Basin Research*, v. 22, p. 79–95, doi:[10.1111/j.1365-2117.2009.00445.x](https://doi.org/10.1111/j.1365-2117.2009.00445.x).
- Gao, Y. F., W. Z. Liu, and X. Y. Ji, 2007, Diagenesis types and features of volcanic rocks and its impact on porosity and permeability in Yingcheng Formation, Songliao Basin (in Chinese with English abstract): *Journal of Jilin University (Earth Science Edition)*, v. 37, no. 6, p. 1251–1257.
- Gao, Y. F., P. J. Wang, R. H. Cheng, G. D. Wang, X. Q. Wan, H. Y. Wu, S. X. Wang, and W. L. Liang, 2009, Description of Cretaceous sedimentary sequence of the first member of the Qingshankou Formation recovered by CCSD-SK1s borehole in Songliao Basin: lithostratigraphy, sedimentary facies, and cyclic stratigraphy: *Earth Science Frontiers*, v. 16, no. 2, p. 314–323, doi:[10.1016/S1872-5791\(08\)60081-0](https://doi.org/10.1016/S1872-5791(08)60081-0).
- Guo, Z. H., P. J. Wang, and C. H. Yin, 2006, Relationship between lithofacies and logging facies of the volcanic reservoir rocks in Songliao Basin (in Chinese with English abstract): *Journal of Jilin University (Earth Science Edition)*, v. 36, no. 5, p. 207–214.
- Hooker, J. N., J. F. W. Gale, L. A. Gomez, S. E. Laubach, R. Marrett, and R. M. Reed, 2009, Aperture-size scaling variations in a low-strain opening-mode fracture set, Cozzette Sandstone, Colorado: *Journal of Structural Geology*, v. 31, p. 707–718, doi:[10.1016/j.jsg.2009.04.001](https://doi.org/10.1016/j.jsg.2009.04.001).
- Huang, H. P., J. Yang, Y. F. Yang, and X. J. Du, 2004, Geochemistry of natural gases in deep strata of the Songliao Basin, NE China: *International Journal of Coal Geology*, v. 58, p. 231–244, doi:[10.1016/j.coal.2003.12.004](https://doi.org/10.1016/j.coal.2003.12.004).
- Huang, Y. L., P. J. Wang, and P. Shu, 2010, Characteristics and formation mechanism of the Cretaceous intermediate and mafic volcanic reservoirs in the Songliao Basin, NE China (in Chinese with English abstract): *Acta Petrologica Sinica*, v. 26, no. 1, p. 82–92.
- Jackson, J. A., 1997, *Glossary of geology*, 4th ed.: Virginia, American Geological Institute, 769 p.
- Lander, R. H., R. E. Laese, and L. M. Bonnell, 2008, Toward more accurate quartz cement models: The importance of euhedral versus noneuhedral growth rates: *AAPG Bulletin*, v. 92, no. 11, p. 1537–1563.
- Laubach, S. E., 2003, Practical approaches to identifying sealed and open fractures: *AAPG Bulletin*, v. 87, no. 4, p. 561–579.
- Laubach, S. E., J. E. Olson, and M. R. Gross, 2009, Mechanical and fracture stratigraphy: *AAPG Bulletin*, v. 93, no. 11, p. 1413–1426, doi:[10.1306/07270909094](https://doi.org/10.1306/07270909094).
- Laubach, S. E., and M. E. Ward, 2006, Diagenesis in porosity evolution of opening-mode fractures, Middle Triassic to Lower Jurassic La Boca Formation, NE Mexico: *Tectonophysics*, v. 419, p. 75–97, doi:[10.1016/j.tecto.2006.03.020](https://doi.org/10.1016/j.tecto.2006.03.020).
- LeMaitre, R. W., et al., 1989, *A classification of igneous rocks and glossary of terms*: London, Blackwell, 193 p.
- Lenhardt, N., and A. E. Götz, 2011, Volcanic settings and their reservoir potential: An outcrop analog study on the Miocene Tepoztlán Formation, Central Mexico: *Journal of Volcanology and Geothermal Research*, v. 204, p. 66–75, doi:[10.1016/j.jvolgeores.2011.03.007](https://doi.org/10.1016/j.jvolgeores.2011.03.007).
- Levin, L. E., 1995, Volcanogenic and volcanoclastic reservoir rocks in Mesozoic-Cenozoic island arcs: examples from the Caucasus and the NW Pacific: *Journal of Petroleum Geology*, v. 18, no. 3, p. 267–288, doi:[10.1111/j.1747-5457.1995.tb00906.x](https://doi.org/10.1111/j.1747-5457.1995.tb00906.x).
- Li, J. K., W. Liu, and L. B. Song, 2006, A study of hydrocarbon generation conditions of deep source rocks in Xujiaweizi fault depression of the Songliao Basin (in Chinese with English abstract): *Natural Gas Industry*, v. 26, no. 6, p. 21–24.
- Li, C. Q., Y. M. Pang, H. L. Chen, and H. H. Chen, 2006, Gas charging history of the Yingcheng Formation igneous reservoir in the Xujiaweizi rift, Songliao Basin, China: *Journal of Geochemical Exploration*, v. 89, p. 210–213.
- Liu, W. Z., Y. L. Huang, Y. M. Pang, and P. J. Wang, 2010, Diagenesis of intermediate and mafic volcanic rocks of Yingcheng Formation (K₁y) in the Songliao Basin: sequential crystallization, amygdule filling and reservoir effect

- (in Chinese with English abstract): *Acta Petrologica Sinica*, v. 26, no. 1, p. 158–164.
- Magara, K., 2003, Volcanic reservoir rocks of northwestern Honshu Island, Japan, in N. Petford and K. J. W. McCaffrey, eds., *Hydrocarbons in crystalline rocks: Geological Society (London) Special Publication 214*, p. 69–81.
- Olson, J. E., S. E. Laubach, and R. H. Lander, 2009, Natural fracture characterization in tight gas sandstones: Integrating mechanics and diagenesis: *AAPG Bulletin*, v. 93, no. 11, p. 1535–1549, doi:[10.1306/08110909100](https://doi.org/10.1306/08110909100).
- Philip, Z. G., J. W. Jennings, J. E. Olson, S. E. Laubach, and J. Holder, 2005, Modeling coupled fracture-matrix fluid flow in geomechanically simulated fracture networks: *Society of Petroleum Engineers Reservoir Evaluation and Engineering*, v. 8, p. 300–309, doi:[10.2118/77340-PA](https://doi.org/10.2118/77340-PA).
- Pollard, D. D., and A. Aydin, 1988, Progress in understanding jointing over the past century: *Geological Society of America Bulletin*, v. 100, p. 1181–1204, doi:[10.1130/0016-7606\(1988\)100<1181:PIUJOT>2.3.CO;2](https://doi.org/10.1130/0016-7606(1988)100<1181:PIUJOT>2.3.CO;2).
- Rowe, M. C., B. S. Ellis, and A. Lindeberg, 2012, Quantifying crystallization and devitrification of rhyolites by means of X-ray diffraction and electron microprobe analysis: *American Mineralogist*, v. 97, p. 1685–1699, doi:[10.2138/am.2012.4006](https://doi.org/10.2138/am.2012.4006).
- Schutter, S., 2003, Occurrences of hydrocarbons in and around igneous rocks, in N. Petford and K. J. W. McCaffrey, eds., *Hydrocarbons in crystalline rocks: Geological Society (London) Special Publication*, v. 214, p. 35–68.
- Sruoga, P., and N. Rubinstein, 2007, Processes controlling porosity and permeability in volcanic reservoirs from the Australand Neuquén Basins, Argentina: *AAPG Bulletin*, v. 91, no. 1, p. 115–129.
- Steward, A. L., and J. McPhie, 2006, Facies architecture and Late Pliocene-Pleistocene evolution of a felsic volcanic island, Milos, Greece: *Bulletin of Volcanology*, v. 68, p. 703–726, doi:[10.1007/s00445-005-0045-2](https://doi.org/10.1007/s00445-005-0045-2).
- Sun, X. M., D. F. Zhu, and C. Q. Zheng, 2007, Feature, epoch and reservoir significance of the Mesozoic faults at the eastern margin of the Songliao Basin (in Chinese with English abstract): *Journal of Jilin University (Earth Science Edition)*, v. 37, no. 6, p. 1055–1063.
- Tang, H. F., Y. M. Pang, and W. H. Bian, 2008, Quantitative analysis on reservoirs in volcanic edifice of Lower Cretaceous Yingcheng Formation in Songliao Basin (in Chinese with English abstract): *Acta Petrologica Sinica*, v. 29, no. 6, p. 841–852.
- Tang, H. F., P. J. Wang, and C. J. Jiang, 2007, Seismic characters of volcanic facies and their distribution relation to deep faults in Songliao Basin (in Chinese with English abstract): *Journal of Jilin University (Earth Science Edition)*, v. 37, no. 3, p. 73–78.
- Tomaru, H., Z. L. Lu, U. Fehn, and Y. Muramatsu, 2009, Origin of hydrocarbons in the Green Tuff region of Japan: ^{129}I results from oil field brines and hot springs in the Akita and Niigata Basins: *Chemical Geology*, v. 264, p. 221–231, doi:[10.1016/j.chemgeo.2009.03.008](https://doi.org/10.1016/j.chemgeo.2009.03.008).
- Wang, P. J., et al., 2007c, Establishment of outcrop system and geo-transects of the Songliao Basin (in Chinese): Daqing Oilfield Company Ltd, Report (312 p) and Atlas (214 figures and 36 tables) of the within-company open file.
- Wang, P. J., S. M. Chen, and W. Z. Li, 2010, Chronology, petrology and geochemistry of the Cretaceous crypto-explosive breccia-bearing volcanic rocks: implication for volcanic reservoir and tectonics of the Songliao Basin, NE China (in Chinese with English abstract): *Acta Petrologica Sinica*, v. 26, no. 1, p. 33–46.
- Wang, P. J., Y. L. Chi, and W. Z. Liu, 2003, Volcanic facies of the Songliao Basin: classification, characteristics and reservoir significance (in Chinese with English abstract): *Journal of Jilin University (Earth Science Edition)*, v. 33, no. 4, p. 449–456.
- Wang, C. S., Z. Q. Feng, and P. J. Wang, 2014, Initial report of the Cretaceous continental scientific drilling project (SK-1) of the Songliao Basin, NE China (in Chinese and English): Beijing, Science Press, 1100 p.
- Wang, P. J., Y. F. Gao, and Y. G. Ren, 2009, $^{40}\text{Ar}/^{39}\text{Ar}$ age and geochemical features of mugearite from the Qingshankou Formation: significances for basin formation, hydrocarbon generation and petroleum accumulation of the Songliao Basin in Cretaceous (in Chinese with English abstract): *Acta Petrologica Sinica*, v. 25, no. 5, p. 1178–1190.
- Wang, X. B., Z. Q. Guo, J. C. Tuo, H. Y. Guo, Z. X. Li, and S. G. Zhuo, 2009, Abiogenic hydrocarbons in commercial gases from the Songliao Basin, China: *Science in China Series D-Earth Sciences*, v. 52, no. 2, p. 213–226, doi:[10.1007/s11430-009-0015-1](https://doi.org/10.1007/s11430-009-0015-1).
- Wang, P. J., W. Z. Liu, S. X. Wang, and W. H. Song, 2002a, $^{40}\text{Ar}/^{39}\text{Ar}$ and K/Ar dating on the volcanic rocks in the Songliao Basin, NE China: constraints on stratigraphy and basin dynamics: *International Journal of Earth Sciences*, v. 91, p. 331–340, doi:[10.1007/s005310100219](https://doi.org/10.1007/s005310100219).
- Wang, P. J., Y. M. Pang, and H. F. Tang, 2007b, The characteristics of the paleo-volcanic edifice of Yingcheng Formation, Cretaceous, Songliao Basin (in Chinese with English abstract): *Journal of Jilin University (Earth Science Edition)*, v. 37, no. 6, p. 1064–1073.
- Wang, P. J., Y. G. Ren, X. L. Shan, S. B. Sun, C. B. Wan, and W. H. Bian, 2002b, The Cretaceous volcanic succession around the Songliao Basin, NE China: relationship between volcanism and sedimentation: *Geological Journal*, v. 37, no. 2, p. 97–115.
- Wang, P. J., X. A. Xie, and M. Frank, 2007a, The Cretaceous Songliao Basin: volcanogenic succession, sedimentary sequence and tectonic evolution, NE China: *Acta Petrologica Sinica (English Edition)*, v. 81, no. 6, p. 801–811.
- Witte, J., M. Bonora, C. Carbone, and O. Oncken, 2012, Fracture evolution in oil-producing sills of the Rio Grande valley, northern Neuquén Basin, Argentina: *AAPG Bulletin*, v. 96, no. 7, p. 1253–1277, doi:[10.1002/\(ISSN\)1099-1034](https://doi.org/10.1002/(ISSN)1099-1034).
- Wu, Y. X., P. J. Wang, and L. Yan, 2010, Quantitative modelling and application of volcanic facies of Lower Cretaceous Yingcheng Formation of the Songliao Basin (in Chinese with English abstract): *Acta Petrologica Sinica*, v. 26, no. 1, p. 73–81.
- Xi, D. P., X. Q. Wan, Z. Q. Feng, S. Li, Z. H. Feng, J. Z. Jia, X. Jing, and W. M. Si, 2011, Discovery of Late Cretaceous

- foraminifera in the Songliao Basin: Evidence from SK-1 and implications for identifying seawater incursions: *Chinese Science Bulletin*, v. 56, no. 3, p. 253–256.
- Xu, S., S. Nakai, H. Wakita, and X. B. Wang, 1995, Mantle-derived noble gases in natural gases from Songliao Basin, China: *Geochimica et Cosmochimica Acta*, v. 59, no. 22, p. 4675–4683, doi:[10.1016/0016-7037\(95\)00301-0](https://doi.org/10.1016/0016-7037(95)00301-0).
- Zheng, C. Q., Z. S. Xu, and P. J. Wang, 2007, Geological characteristics and hydrocarbon reservoir significance of the diabase porphyrite at the Shanghewan area, southeast uplift of the Songliao Basin, NE China (in Chinese with English abstract): *Journal of Jilin University (Earth Science Edition)*, v. 37, no. 6, p. 1097–1103.